MATERIALS CHEMISTRY FRONTIERS

CCS 中国化学会 CHINESE CHEMICAL SOCIETY

ICCAS

ROYAL SOCIETY OF CHEMISTRY

REVIEW

View Article Online
View Journal | View Issue

Cite this: *Mater. Chem. Front.*, 2023, **7**, 789

The nonhalides in perovskite solar cells

Shurong Wang,[a] Cheng Wu,[a] Huanhuan Yao,[a] Liming Ding [b] and Feng Hao *[a]

Received 8th November 2022,
Accepted 30th December 2022

DOI: 10.1039/d2qm01147f

rsc.li/frontiers-materials

Recently, halide perovskite solar cells (PSCs) have accomplished the most remarkable progress in emerging photovoltaic technology. However, their poor stability hinders the route to commercialization. Notably, the high chemical activity of halides such as I^- and Br^- and the formed halide-related vacancy defects lead to the instability of PSCs. In spite of the importance of X-site anions, more and more works have been devoted to the polyatomic pseudohalides and superhalogens in perovskites. In this context, this review will focus on the basic understanding of the structural and photoelectric properties of pseudohalides and superhalogens. We comprehensively summarize the current research progress of SCN^-, $HCCO^-$, Ac^-, BF_4^-, BH_4^-, and PF_6^- anions to realize high structurally stable perovskites and related solar cells. Based on these observations, some perspectives on future efforts toward achieving highly stable PSCs are proposed and discussed.

1. Introduction

Perovskite solar cells (PSCs) have driven much interest in the development of photovoltaic devices since they first emerged in 2009.[1,2] The hybrid organic–inorganic halide perovskites act as a classical solar absorber material. Their great merits such as high carrier mobility, high absorption coefficient, low carrier recombination rate, low exciton binding energy, high defect tolerance, and tunable band-gap properties enabled an outstanding performance within a decade.[3–6] The certified power conversion efficiency (PCE) has been pushed to 25.7% with superior long-term operational stability.[7]

In general, the halide perovskite has a ABX_3 scaffold, where the A site denotes a monovalent cation (such as $CH_3NH_3^+$ (MA^+), $CH(NH_2)_2^+$ (FA^+), and Cs^+), the B site denotes a divalent metal cation (such as Pb^{2+} and Sn^{2+}), and the X site denotes a monovalent anion (such as I^-, Cl^-, and Br^-).[8] The corner-shared $[BX_6]^{4-}$ octahedra form a cuboctahedral cavity to accommodate the A site that satisfies the three-dimensional (3D) perovskite structure. The electronic and optical properties of the halide perovskite show a great relationship to the composition and structural variations. The exploration of the possible range of A-site cations has been widely investigated. The alternative A-site cations to yield the 3D perovskite lattice only are Cs^+, FA^+, and MA^+. Other large organic spacer cations (such as PEA^+

[a] School of Materials and Energy, University of Electronic Science and Technology of China, Chengdu, 611731, China. E-mail: haofeng@uestc.edu.cn
[b] Center for Excellence in Nanoscience (CAS), Key Laboratory of Nanosystem and Hierarchical Fabrication (CAS), National Center for Nanoscience and Technology, Beijing, 100190, China

Shurong Wang

Shurong Wang is currently pursuing her PhD under the supervision of Prof. Feng Hao at the School of Materials and Energy, University of Electronic Science and Technology of China. She received her BS in Applied Chemistry (2017) and ME in Environmental Engineering (2020) from Nanjing University of Information Science and Technology. Her current research focuses on component engineering and defect engineering for lead-free perovskite solar cells.

Cheng Wu

Cheng Wu received his Master's degree from Jiangsu University in 2021. Now he pursuing his PhD supervised by Prof. Feng Hao at the University of Electronic Science and Technology of China. His current research interest mainly focuses on developing highly efficient organic interlayer for lead-free perovskite solar cells.

($C_6H_5(CH_2)_2NH_3^+$), BA^+ ($CH_3(CH_2)_3NH_3^+$), or EDA^{2+} ($(CH_2)_2(NH_3)_2^{2+}$)) could be incorporated into perovskites to form a low-dimensional structure like the RP (Ruddlesden–Popper) phase with a formula of $A'_2A_{n-1}B_nX_{3n+1}$ or the DJ (Dion–Jacobson) phase with a $A'A_{n-1}B_nX_{3n+1}$ framework. However, a preferred vertical orientation of a low-dimensional perovskite is hard to achieve owing to its different quantum well thickness with different n values. The small n-value perovskite is more likely to orient parallel to the substrate, and the high n-value perovskite tends to achieve a vertical orientation.[9]

In addition, the Pb^{2+} of the B-site cation has high toxicity, which is very concerning in terms of environmental and human health concerns. Other metal cations with similar electron configurations in the IVA/VA group, such as Sn^{2+}, Ge^{2+}, Sb^{3+}, Bi^{3+}, Ag^+, Cu^+, and Au^+, still show poor performance.[10,11] Meanwhile, I^-, Cl^-, and Br^- are the most widely used X-site anions, which react with BX_2 to form the ABX_3 perovskite materials. However, the halide anion of I^- shows high chemical activity and the corresponding I^- vacancy defects could form easily. The existing I^- vacancy defects have a negative impact on the device stability owing to the unwanted increase in ion conductivity.[12] Partial substitution of I^- by Br^- could tune the band gap and improve the structural stability. As for Cl^-, the Cl^- incorporation could affect the nucleation and crystallization of the perovskite film, although it is too small to incorporate into a perovskite lattice.[13]

Other efforts have also been reported to form stable perovskites such as SCN^- (thiocyanate), Ac^-, $HCOO^-$, BF_4^- (tetrafluoroborate), and PF_6^- (hexafluorophosphate).[2,14–17] Yan *et al.* delivered efficient and stable PSCs by using $Pb(SCN)_2$ in a perovskite precursor.[18] This SCN^--modulated perovskite film is a high-quality perovskite film with increased grain size. Other studies with the $HCCO^-$ anion have also been investigated. Estroff and Abate *et al.* enabled an excellent coverage and large crystal domains with the use of MAHCOO.[19,20] Grätzel *et al.* used FAHCOO to suppress the anion-vacancy defects and nonradiative recombination in $FAPbI_3$ perovskites.[2] The BF_4^- anion plays a key role in improving charge extraction in the interface and reducing the voltage deficiency.[17,21] An appropriate amount of PF_6^- addition could stabilize the Pb–X–Pb octahedral frame in perovskites, which is beneficial for the less nonradiative recombination and enlarged carrier lifetime.[21] Notably, these nonhalides have shown various functions in realizing superiorly stable and high-performance PSCs. However, the effects of anions beyond I^-, Cl^-, and Br^- on perovskites have yet to be fundamentally understood.

In this review, we first describe the basic understanding of the structural and photoelectric properties in nonhalides including pseudohalides and superhalogens. Then we comprehensively summarize the current research progress of SCN^-, $HCCO^-$, Ac^-, BF_4^-, BH_4^-, and PF_6^- anions to realize highly structurally stable perovskite materials and devices. Their functions in perovskites are systematically summarized, including the strong interaction with perovskites, nucleation and growth, phase stability, efficiency, stability enhancement, and defect passivation. Finally, based on these observations, we propose our perspectives on the future efforts towards achieving highly stable PSCs and devices.

Huanhuan Yao

Huanhuan Yao is currently pursuing her PhD under the supervision of Prof. Feng Hao at the School of Materials and Energy, University of Electronic Science and Technology of China. She received her BS in physics (2019) from Northwest Normal University and ME in materials science and engineering (2022) from Lanzhou University. Her current research focuses on lead-free perovskite solar cells.

Liming Ding

Liming Ding achieved his PhD degree from the University of Science and Technology of China. He started his research on OSCs and PLEDs in Olle Inganäs Lab in 1998. Then, he worked with Frank Karasz and Tom Russell at PSE, UMASS Amherst. He joined Konarka as a Senior Scientist in 2008. In 2010, he joined the National Center for Nanoscience and Technology as a Full Professor. His research interests include perovskite solar cells, organic solar cells and photodetectors.

Feng Hao

Feng Hao received his PhD from Tsinghua University in 2012. Then he moved to Northwestern University as a postdoc in the Department of Chemistry. He has been a full professor at the School of Materials and Energy, University of Electronic Science and Technology of China since 2017. His research focuses on perovskite solar cells and photonic materials.

2. Overview of nonhalide anions

To obtain a typical 3D perovskite crystal, the crystallographic stability is determined by Goldschmidt's tolerance criteria (t) and octahedral factor (μ):[22]

$$t = \frac{R_A + R_X}{\sqrt{2}(R_B + R_X)} \quad (1)$$

$$\mu = \frac{R_B}{R_X} \quad (2)$$

where R_A, R_B, and R_X are the ion radii of A, B, and X site ions. To form a stable perovskite crystal with a 3D framework, the value of t and μ must be in the range of $0.81 < t < 1.11$, and $0.44 < \mu < 0.90$, respectively.[23,24]

The X-site anions are not limited to the three halides (I^-, Cl^-, and Br^-), alternatively, it can be defined as negative monovalent anions or polyatomic anions with −1 charge. The ion radius shows a decreasing trend: R_{Cl}^- (181 pm) < R_{Br}^- (196 pm) < R_I^- (220 pm). There are two types of nonhalides in perovskites (Fig. 1a). On the one hand, the stable pseudohalides (*e.g.* SCN^-, Ac^-, and $HCOO^-$) have gained much attention. SCN^- has a similar ion radius to I^- (217 pm for SCN^-).[25] The linear Lewis structure of SCN^- showed stable resonance, rendering a strong Lewis acid-base interaction with Pb^{2+} or Sn^{2+} when considering the long pairs of electrons from N and S atoms.[26,27] $HCOO^-$ has a stronger bonding with FA^+ than BF_4^-, I^-, Br^-, and Cl^- owing to the hydrogen bonding.[2] The most deleterious defects of I^- vacancies can be eliminated with $HCOO^-$. On the other hand, superhalogens such as BH_4^-, PF_6^-, and BF_4^- have a higher electronegative and electron affinity than halides.[28,29] The use of superhalogens greatly enhances the structural stability *via* partial substitution of halides. Therefore, the recent emergence of pseudohalides or superhalogens can significantly mitigate the defect-related instability in PSCs.

2.1 Pseudohalides

The effective ion radii of polyatomic anions usually satisfy the following criteria:[30]

$$R_{Xeff} = \sqrt[3]{\text{volume} \times \frac{3}{4\pi}} \quad (3)$$

It is reliable to apply a general comparison of the relative ion size of the pseudohalides. To satisfy Goldschmidt's tolerance criteria, the range of A-site cations increased with the size of X-site anions (Fig. 1b). The maximum value of spherical X anions is R_X = 2.42 R_B ($\mu \geq 0.414$) to stabilize the $[BX_6]^{4-}$ octahedral. Therefore, the X-site anions with a size up to 287 pm can form a stable $[BX_6]^{4-}$ octahedral, which allows the size of A sites up to 288 pm in lead perovskites. For nonspherical X anions, the effective R_X may be greater than 2.42 R_B, which depends on how the ligands of the X site coordinate to the B site.[30] The pseudohalides mainly contain N_3^- (azides),[31] CN^- (cyanides),[32] $N(CN)_2^-$ (dicyanamides),[33] SCN^-,[29] $HCOO^-$, $^2Ac^-$,[34] and I_3^- (triiodides).[35] Beside the Pb- and Sn-based perovskites, the perovskite-like lattice can accommodate other B-site cations, such as $[(CH_3)_4N]Mn(N_3)_3$, $Ni(NH_3)(CN_2)\cdot C_6H_6$, $[NH_3(CH_2)_7NH_3]_2Au_2I_6(I_3)_2$, $MAMn(HCOO)_3$, *etc.*[31,32,35,36] The polyatomic $HCOO^-$ anion has a similar size to Br^- and a planar structure.

SCN^- has been extensively investigated for improving the stability of perovskites. Yan *et al.* calculated the crystal structure of $MAPbI_x(SCN)_{3-x}$ perovskites by density functional theory (DFT) calculation (Fig. 1c and d).[37] The incorporation of the SCN^- group delivered a thermodynamically stable lattice with a pseudo-orthorhombic framework.[37] Ganose *et al.* also verified

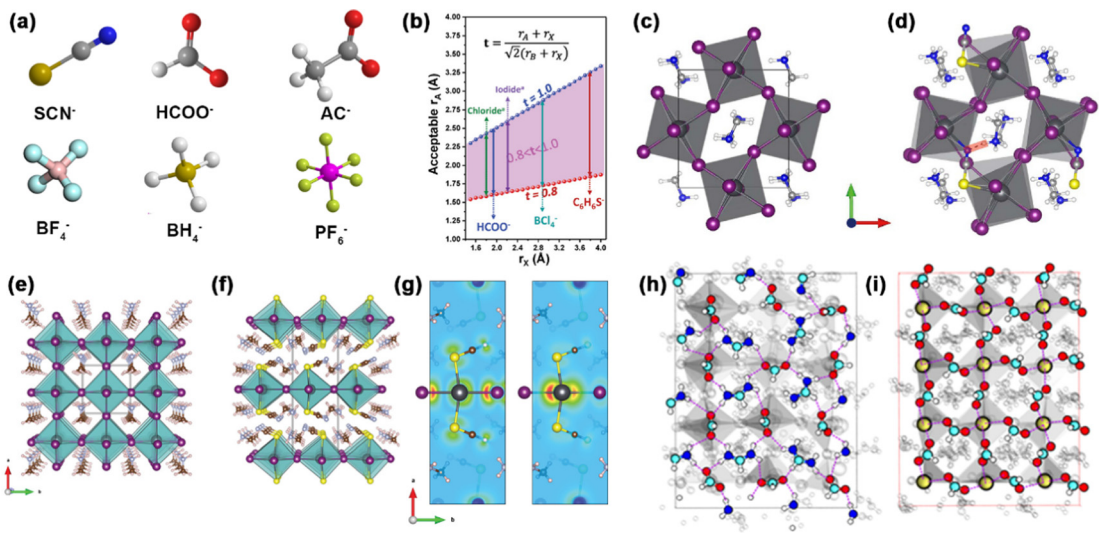

Fig. 1 (a) The structure of nonhalides in perovskites. (b) The range of ion radii of A-site and X-site ions that satisfy $0.81 < t < 1.11$. Reproduced with permission.[30] Copyright 2019, Wiley-VCH Publications. Crystal structure of (c) $MAPbI_3$ and (d) $MAPb(SCN)I_{3-x}$. Reproduced with permission.[37] Copyright 2015, Springer Nature. Crystal structure of (e) $MAPbI_3$ and (f) $MA_2Pb(SCN)_2I_2$. (g) Charge density isosurface of VBM (left) and CBM (right) in $MA_2Pb(SCN)_2I_2$. Reproduced with permission.[38] Copyright 2015, American Chemical Society. Top view of surface atoms in (h) the FA^+-terminated surface and (i) Pb^{2+}-terminated surface. Reproduced with permission.[2] Copyright 2020, Springer Nature.

the thermodynamically stable structure in 2D hybrid perovskites (Fig. 1e and f).[38] The 2D $MA_2Pb(SCN)_2I_2$ layered perovskite has a space group of $Pnm2_1$, where the Pb atom octahedrally coordinated to two apical (or *trans*) S-bonded SCN^- anions and four axial I^- anions. Meanwhile, the MA^+ molecule was sandwiched between the layers, forming an orthorhombic pattern like the K_2NiF_4 compound. SCN^- has a great role in bonding, where the valence band maximum (VBM) and conduction band minimum (CBM) is determined by Pb 6p-I 5p and Pb 6p orbitals, respectively (Fig. 1g). There is also a small contribution of S 3p and N 2p in the SCN^- in VBM. $HCOO^-$ was rarely reported in the inorganic–organic hybrid perovskites. Instead, it can coordinate with Mn^{2+} cations and form a $MAMn(HCOO)_3$ structure. It plays a significant role in eliminating halide vacancy defects and alleviates the adverse ionic conductivity of perovskites (Fig. 1h and i).[2]

2.2 Superhalogens

Superhalogens have a higher electron affinity than halides, such as BH_4^-, BF_4^-, and PF_6^-.[39] Ogale *et al.* first applied them to solid-state dye-sensitized solar cells as a component of the X site by using $MABF_4$.[40] BF_4^- and PF_6^- could partially substitute I^- to form stable organic–inorganic perovskite superlattices, which provide a large variety of possibility to expand the possible perovskite formulations.[41,42] The addition of BF_4^- in $FAPbI_3$ could enhance the formation energy of FA^+-related vacancies to improve the structural stability.[42] BF_4^- has a higher electronegativity than the F^-, implying that the bonding between BF_4^- and its neighboring Pb atom would be more ionic. Li *et al.* calculated the VBM and CBM of the minimum-energy superlattice structures of $(FAPbI_3)_3/CsPbI_2BF_4$, $(MAPbI_3)_3/CsPbI_2BF_4$, $(FAPbI_3)_3/MAPbI_2BF_4$, and $(CsPbI_3)_3/MAPbI_2BF_4$ (Fig. 2a–d and e–h).[43] The charge density in $(MAPbI_3)_3/CsPbI_2BF_4$, $(FAPbI_3)_3/MAPbI_2BF_4$ illustrated that the VBM and CBM states were distinctly separated in space and had no slap. While the charge density of VBM and CBM value in $(FAPbI_3)_3/CsPbI_2BF_4$ and $(CsPbI_3)_3/MAPbI_2BF_4$ had a slight overlap on the Pb atoms and was far away from the $CsPbI_2BF_4$ and $MAPbI_2BF_4$ layers. They also calculated the layers of $FAPbI_3$, $MAPbI_3$, and $CsPbI_3$ from one to three along the direction of the base vector *a*. The complete separation of charge density in VBM and CBM states is beneficial to the electrons/holes collection owing to the effective electrons/holes restriction in different atomic layers. Increasing the number of layers could solve the incomplete separation of the charge density of the VBM and CBM states.

For perovskite superlattices, the electrons are distributed in the potential well and holes in the potential barrier. For instance, the superlattice with BF_4^- is a type-II superlattice.[43] The great spatial separation of electrons/holes with superhalogens has a significant effect on carrier transport and collection. In addition, Hendon *et al.* simulated the crystal structure with VBM and CBM states of $CsPbI_{3-x}(PF_6)_x$ and $CsPbI_{3-x}(BF_4)_x$ perovskites as shown in Fig. 2d–p.[41] Compared to the octahedral $CsPbI_3$ perovskite ($pm3m$), $CsPb(PF_6)_3$ maintained a cubic lattice by the linear coordination through the axial termini. $CsPb(BF_4)_3$ had C_s symmetry with $C1m1$ space group. The B–F bond in $CsPb(BF_4)_3$ was not inline owing to the linear

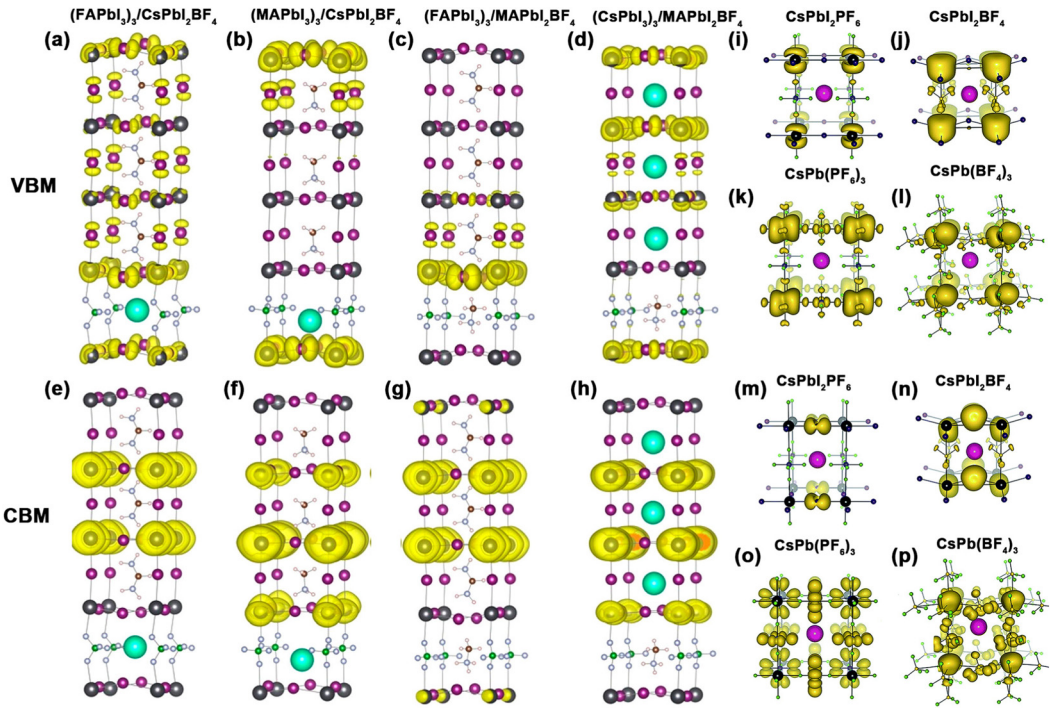

Fig. 2 Charge density in the (a–d) VBM and (e–h) CBM states of $(FAPbI_3)_3/CsPbI_2BF_4$, $(MAPbI_3)_3/CsPbI_2BF_4$, $(FAPbI_3)_3/MAPbI_2BF_4$, and $(CsPbI_3)_3/MAPbI_2BF_4$, respectively. Reproduced with permission.[43] Copyright 2020, American Chemical Society. Charge density in the (i–l) VBM and (m–p) CBM states of $CsPbI_2PF_6$, $CsPbI_2BF_4$, $CsPb(PF_6)_3$, and $CsPb(BF_4)_3$, respectively. Reproduced with permission.[41] Copyright 2015, The Royal Society of Chemistry.

coordination occurring by two edges of the tetrahedron. As for BH_4^-, it consists of two elements and has one extra electron satisfying the electronic shell closure.[44] In addition to the suppression of I^- vacancy defects, BH_4^- has a strong dihydrogen interaction with MA^+. The existence of BH_4^- could substitute the I^- anion or compensate for the I^- vacancy defects.[45,46]

3. SCN^-

3.1 Acting as an X-site anion in halide perovskites

Bilaji *et al.* first used a pseudohalide salt of $Pb(SCN)_2$ and $Pb(NO_3)_2$ with MAI vapors through a sequential vapor-assisted solution process[47] to achieve the ion exchange of SCN^- and I^-, or NO_3^- and I^-, respectively. Yan *et al.* used $Pb(SCN)_2$ precursor and prepared a high-quality $MAPbI_{3-x}SCN_x$ perovskite film.[37] The S and N atoms with long pairs of electrons in SCN^- have strong interaction with Pb atoms, which in turn stabilized the frame structure of $MAPbI(SCN)_2$. Jiang *et al.* compared the X-ray diffraction (XRD) patterns of $MAPbI_3$ and $MAPbI(SCN)_2$ (Fig. 3a).[48] The characteristic peaks at 14°, 20°, 29°, 32°, and 41° for the $MAPbI(SCN)_2$ film could be indexed to the formed perovskite structure. They designed moisture-tolerance tests *via* the reflection spectrum in Fig. 3b and c. There is no obvious variation in the film color of the $MAPbI(SCN)_2$ film for 0–1.5 h. Moreover, the black $MAPbI(SCN)_2$ film still maintained the original morphology for months in air with 40% relative humidity. After exposure to air with 95% humidity, the $MAPbI(SCN)_2$ remained the stable perovskite structure with an E_g of 1.532 eV. The resulting PSC device with $MAPbI(SCN)_2$ delivered a PCE of 8.3%. Yan *et al.* indicated that adding $Pb(SCN)_2$ below 1.0 mmol% did not change the E_g value of $FA_{0.8}Cs_{0.2}Pb(I_{0.7}Br_{0.3})_3$ perovskites.[49] Lou *et al.* also illustrated that the pure $CsPb(SCN)_3$ displayed the highest E_g compared with $CsPbBr_3$ and $CsPbI_3$ perovskites.[50] The up-shifted VBM was responsible for the increase of E_g. The strong interaction between SCN^- and Pb^{2+} (like Pb–S, Pb–N, and Pb–C bonds) lead to a rather high-energy anti-bonding orbital when compared to $CsPbBr_3$ and $CsPbI_3$.

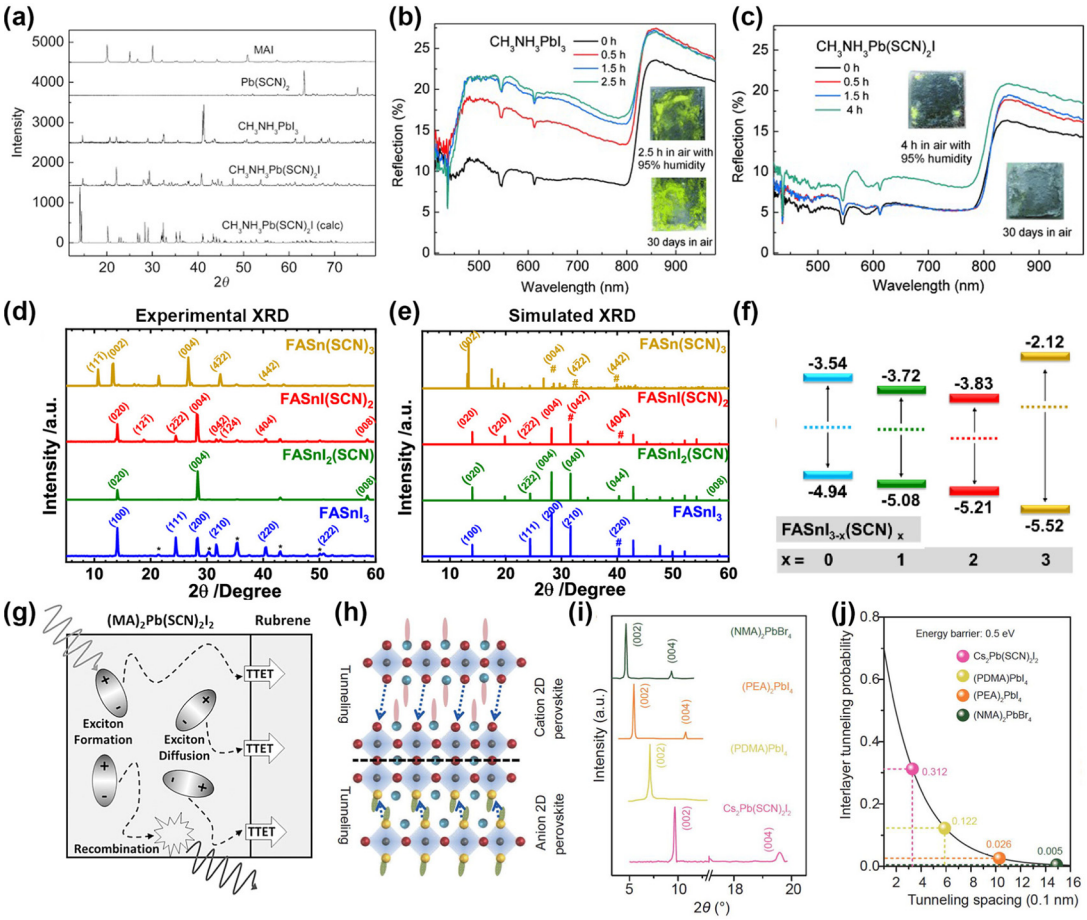

Fig. 3 (a) XRD patterns of $MAPbI_3$ and $MAPbI_2(SCN)$ perovskite films. (b and c) Reflection spectrum with stability tests of $MAPbI_3$ and $MAPbI_2(SCN)$ in the air with 95% humidity. Reproduced with permission.[48] Copyright 2015, Wiley-VCH Publications. (d and e) Experimental and simulated XRD patterns of $FASnI_{3-x}(SCN)_x$ perovskite films. (f) Energy level diagrams of $FASnI_{3-x}(SCN)_x$ perovskites. Reproduced with permission.[52] Copyright 2020, American Chemical Society. (g) Exciton diffusion and triplet-triplet energy transfer at the 2D perovskites/rubrene interface. Reproduced with permission.[55] Copyright 2017, Wiley-VCH Publication. (h) The lattice structure of $Cs_2PbI_2(SCN)_2$ perovskites. (i) XRD patterns of four types of 2D perovskites. (j) Relationship between charge channeling probability and interlayer spacing. Reproduced with permission.[57] Copyright 2021, Springer Nature.

Meanwhile, SCN^- has a strong ionic interaction with Sn^{2+}.[51] Owing to the π-conjugated electron system, the incorporation of SCN^- showed great enhancement in photoelectron transfer.[52,53] Diau *et al.* observed the enhanced structural stability in $FASnI_{3-x}(SCN)_x$ perovskites and a maximum was reached in $FASnI(SCN)_2$.[52] Indeed, SCN^- was deemed as a bridging ligand to construct a stable octahedra framework due to its ambident nucleophilicity. The XRD patterns in Fig. 3d and e showed three main perovskite peaks around 14°, 28°, and 41° in $FASnI_{3-x}(SCN)_x$ perovskites. However, the diffraction peaks of $FASn(SCN)_3$ shifted to smaller angles with the increase of lattice spacing. Similar to the other mixed-halide substitution,[54] adding SCN^- in $FASnI_{3-x}(SCN)_x$ films showed a decreased VBM value when increasing x from 0 to 3 (Fig. 3f). Besides, $FASnI_{3-x}(SCN)_x$ has enhanced oxidation resistance, which is attributed to the enhanced hydrophobicity and strong interaction with Sn^{2+}.

The 2D $(MA)_2Pb(SCN)_2I_2$ perovskites exhibit a photoactive triplet state.[55] After spin-coating rubrene, a small organic molecule, the obvious triplet energy transfer from $(MA)_2Pb(SCN)_2I_2$ to rubrene was observed (Fig. 3g). This phenomenon exhibited unique photophysical behavior with triplet state phosphorescence. Therefore, 2D perovskites with SCN^- have great potential in the use of triplet sensitizer. Moreover, 2D $Cs_2PbI_2(SCN)_2$ shows high thermal stability.[56,57] Meng *et al.* explored the photoelectric properties of $Cs_2PbI_2(SCN)_2$ perovskites.[57] The charge transport across the inorganic layers is determined by the quantum tunneling effect. The space between inorganic layers showed negligible contributions to VBM and CBM. It was observed that $Cs_2PbI_2(SCN)_2$ had a crystal orientation along the [001] direction like $(NMA)_2PbBr_4$, $(PEA)PbI_4$, and $(PDMA)PbI_4$. However, the (002) and (004) peaks shifted to larger angles with decreasing size of the cation or anion (Fig. 3i). Meanwhile, the interlayer tunneling probability of the $Cs_2PbI_2(SCN)_2$ perovskite reached 0.312, which was ten times higher than those of $(NMA)_2PbBr_4$ and $(PDMA)PbI_4$ (Fig. 3j). Large tunneling probability and small interlayer spacing contributed to fast charge transport with high conductivity. Therefore, 2D $Cs_2PbI_2(SCN)_2$ perovskites have super small interlayer spacing and interlayer nano channels, which will promote the charge transport.

Ning *et al.* employed PEAI and $Sn(SCN)_2$ to form 2D $PEA_2Sn_2I_{4-x}SCN_x$ perovskites as an intermediate template for the growth of 3D $CsSnBrI_{2-x}SCN$ perovskites.[58] This approach enabled the preferred out-of-plane growth of a 2D–3D mixed structure with homogeneous inclusion of SCN^- in the 3D $CsSnBrI_{2-x}SCN$ perovskite structure, further contributing to the suppressed defect density and retarded Sn^{2+} oxidation. The pseudohalide-modulated 2D perovskites also show great potential in tuning the electronic properties of perovskites. Liu *et al.* adopt the 2D Sn perovskites with pseudohalide to adjust the electronic and excitonic properties.[59] The 2D $BA_2SnI_2SCN_2$ and BA_2SnI_4 perovskites had the smallest exciton binding energy and effective mass compared with the Pb- and Br-based 2D perovskites. The strong exciton effect in pseudohalide-substituted 2D tin perovskites could enhance PL performance as well as photocurrent when applied in PSCs according to the *J–V* curve.

3.2 Acting as additives in halide perovskites

3.2.1 Amine-type additives

GUASCN (guanidinium thiocyanate). The strong binding affinity of SCN^- could recover the oxidized sites and coordinate with undercoordinated sites to passivate the defects, which cannot be reached by classical halides.[27,60,61] The strong hydrogen bonding between GUA^+ and SCN^- further contributes to the additional stabilization of perovskites. Pham *et al.* elucidated the grain growth mechanism with GUASCN:[62]

$$MAPbI_3 + GUASCN \rightarrow GUAI\ (s) + PbI_2\ (s) + MA\ (g) + HSCN\ (g)\uparrow \quad (4)$$

With the surface treatment of GUASCN, the HSCN gas was expelled from the film rapidly and the formed GUAI, PbI_2, or the $((GUAI)_x(PbI_2)_y)$ compound accumulated at GB as a secondary phase. The MA gas enhanced the de-nucleation rate and solubility of unwanted small $MAPbI_3$ crystals, thus facilitating grain coarsening. Zhu *et al.* proved that adding 7 mol% GUASCN can substantially improve the carrier lifetime up to 1 μs in Sn–Pb perovskite films.[14,63] The calculated surface recombination velocity (S) and carrier diffusion coefficient (D) from the transient reflection (TR) spectrum in Fig. 4a and b illustrated that the fitted S increased from 10–100 cm s^{-1} to 1.0 × 10^2 cm s^{-1}. GUASCN is a common additive to reduce the pinholes and small grains in hybrid halide perovskites. Zhang *et al.* claimed that GUASCN could inhibit the 1D solvate intermediate phase and form high-quality quasi-2D films.[64] The following reaction revealed the potential mechanism:

$$MAPbI_3{\cdot}DMF + yGUASCN \rightarrow y/xPbI_{2-x}SCN_x + (1 - y/x)PbI_2 + MAI + yGUAI + DMF \quad (5)$$

The decomposition products of GUAI and $PbI_{2-x}SCN_x$ enlarged the grain size and enhanced the crystalline quality of thin films. The fitted rapid rise time (τ) by ultrafast transient absorption (TA) spectroscopy in Fig. 4c and d indicated that the perovskite film with GUASCN had faster τ of 4.43 ps, 4.78 ps, and 107.90 ps for n = 3, 4, and 5, respectively, where the control films had τ of 0.15 ps (n = 2), 6.78 ps (n = 3), 8.86 ps (n = 4), and 13.21 ps (n = 5), respectively. Therefore, GUASCN significantly improved the energy/charge transfer efficiency due to a suppressed recombination center and effective energy/charge transfer. A similar approach was also reported in colloidal quantum dot (CQD) photovoltaics.[65] The bidentate nature of SCN^- leads to improved electronic coupling in the CQD matrix.[2,66,67] GUASCN has nearly zero dipole moment, thus benefiting charge transport. By surface reconstruction, GUASCN played a key role in surface passivation *via* epitaxial surface bridges with CQD. The oxidized species were eliminated with GUASCN by substituting Pb–O to the Pb–SCN bond (Fig. 4e). The upshifted C≡N stretch in Fig. 4f proved the surface reconstruction between the SCN^- and CQD surface.

NH_4SCN. The pseudohalide SCN^- anion could drive the secondary formation of thin films as the intermediate catalyst, therefore ensuring the composition purity both in the original

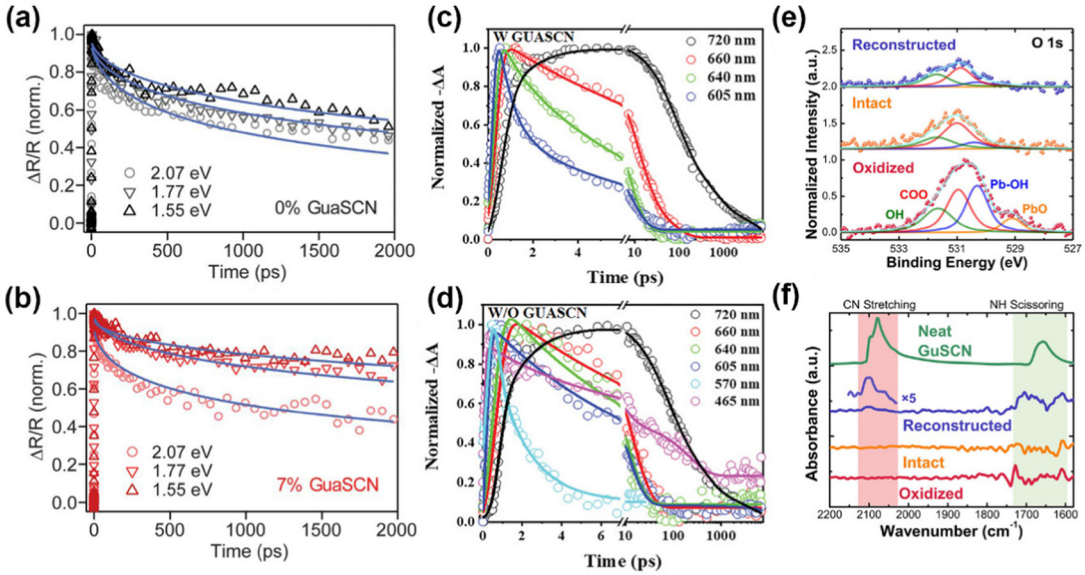

Fig. 4 (a and b) TA spectra of 0% and 7% GUASCN addition under different pump photon energies. Reproduced with permission.[14] Copyright 2019, American Association for the Advancement of Science. (c and d) TA kinetics of quasi-2D perovskites without/with GUASCN. Reproduced with permission.[64] Copyright 2022, Wiley-VCH Publication. (e) XPS peaks of O 1s. (f) FTIR spectra of the CQD solids and neat GUASCN. Reproduced with permission.[65] Copyright 2022, American Chemical Society.

films and final polycrystals. The SCN^- group in NH_4SCN was not incorporated into the perovskite lattice in the final-state perovskite films. Jen *et al.* proposed the recrystallization process with NH_4SCN:[68]

$$MAPbI_3 + SCN^- \rightarrow PbI_6^{4-} + MA^+{\cdot}SCN^- \quad \text{(dipping)} \qquad (6)$$

$$MA^+{\cdot}SCN^- + NH_4^+ \rightarrow MA^+ + HSCN\,(g)\uparrow + NH_3\,(g)\uparrow \quad \text{(annealing)} \qquad (7)$$

$$PbI_6^{4-} + MA^+ \rightarrow MAPbI_3 \qquad (8)$$

Therefore, the undissolved polycrystals could recrystallized and form new $MAPbI_3$ crystal. The SCN^- anions in NH_4SCN can strongly interact with Pb^{2+}/Sn^{2+} and the organic cations, where NH_4^+ cations could interact with $[PbI_6]^{4-}$ or $[SnI_6]^{4-}$.[68–70] Chou *et al.* revealed the role of in 2D tin perovskites by time-of-flight secondary ion mass spectrometry (ToF-SIMS) to detect the location of SCN^- anions (Fig. 5a and b).[71] The positive and negative signals of Sn, I, SCN, and TEA (2-thiophene-ethylammonium) were located at the same region, which indicated the SCN can coordinate with Sn^{2+}. Zhang *et al.* investigated the NH_4SCN concentration in the orientation and crystallinity of 2D $(PEA)_2(MA)_{n-1}Pb_nI_{3n+1}$ films (Fig. 5c–e).[72] The 2D perovskites in the absence of NH_4SCN showed random orientation and weak preferential orientation, while the film with 2% SCN^- had sharp and discrete Bragg spots and a considerable increase in orientation.

MASCN and FASCN. MASCN can significantly reduce the reaction activity *via* the strong interaction with Sn^{2+}/Pb^{2+}.[73–75] For instance, Lian *et al.* proved that MASCN can retard the reaction between FAI and Sn^{2+} and also suppress the Sn^{2+} oxidation.[74] Zhang *et al.* added 5% MASCN into $(PA)_2(MA)_4Pb_5I_{16}$ (PA is *n*-pentylammonium) perovskite precursor to regulate the phase distribution.[75] The TA patterns in Fig. 5f at various delay times indicated that the peaks at 570 nm, 606 nm, 640 nm, 666 nm, and 720 nm attributed to $n = 2$, $n = 3$, $n = 4$, $n = 5$, and 3D-like phases in $(PA)_2(MA)_4Pb_5I_{16}$ film, respectively. The $n = 2$ phase disappeared and the 3D-like phase enhanced remarkably in MASCN-modified films (Fig. 5g), further proving that the perovskite film with SCN^- obtained a high *n*-value phase and large grain. Moreover, the improved water contact implied great hydrophobicity of perovskite films in Fig. 5h. The XRD patterns in pseudohalide-induced perovskite films had barely changed 2D phases after storing for 60 days. Different from the previous report, Grätzel *et al.* used MASCN and FASCN vapor to achieve phase transition and obtain stable black-phase $FAPbI_3$ perovskites.[76] The formed corner-sharing Pb–I–SCN structures at the interface could maintain kinetically stable perovskites. The vapor-treated $FAPbI_3$ devices maintained 94.4% PCE of the original value after 500 h testing at the maximum power point (MPP).

PEASCN and TEASCN. Compared to pure PEAI treatment, the PEASCN source conformed to a more crystalline film.[77] The PEASCN sample can reach a carrier lifetime of over 2 μs and carrier mobility over 40 $cm^{-2}\ V^{-1}\ s^{-1}$. Khadka *et al.* introduced PEASCN into pure $FASnI_3$ perovskites to achieve defect suppression in the bulk and interface.[78] These polyatomic pseudohalides delivered a high PCE of 9.65% with a V_{oc} of 667 mV in the corresponding devices. Therefore, the PEASCN not only acts as a 2D additive but also as a crystallization regulator. Ning *et al.* synthesized a new pseudohalide molecule TEASCN (TEA is 2-thiopheneethylamine) to construct a bilayer quasi-2D structure on the Sn–Pb perovskite surface.[79] The TEASCN-

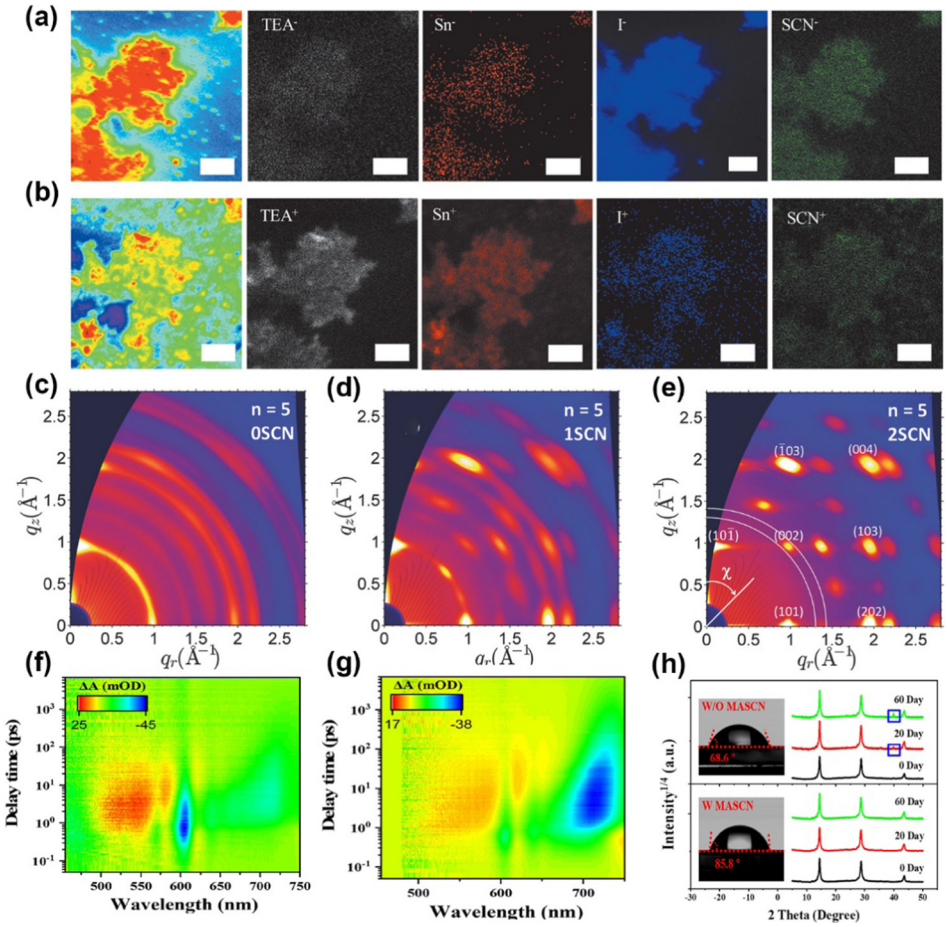

Fig. 5 ToF-SIMS mapping of 2D perovskites with 7% NH_4SCN: (a) negative signals of TEA^-, Sn^-, I^-, and SCN^-; (b) positive signals of TEA^+, Sn^+, I^+, and SCN^+. Reproduced with permission.[71] Copyright 2020, Wiley-VCH Publication. (c–e) 2D GIWAX patterns of 2D perovskite films with various amounts of NH_4SCN. Reproduced with permission.[72] Copyright 2018, Wiley-VCH Publication. TA patterns of $(PA)_2(MA)_4Pb_5I_{16}$ film (f) without and (g) with MASCN. (h) XRD images and contact angle tests with or without MASCN. Reproduced with permission.[75] Copyright 2022, American Chemical Society.

introduced films enabled a high *n*-value (n = 2) phase while the TEAI-introduced films formed a low *n*-value phase of n = 1.

3.2.2 Metal-type additives. KSCN and NaSCN are the most commonly used additives in perovskites.[80–84] Zhang *et al.* used the two additives to improve the microstructure perovskite structure and crystallinity of thin films.[18] The NaSCN treatment could suppress the Br^- vacancies and decreased the surface defect density, thus further increasing the device stability.[82] Besides the effect of SCN^-, K^+ could also passivate defects. Xu *et al.* found that KSCN can enlarge perovskite grains to an average diameter of 11 μm.[81] This attempt enabled the carrier diffusion length to around 25 μm in slot-die-coated perovskite films. Additionally, Cao *et al.* used KSCN as an interlayer between PEDOT:PSS and $FA_{0.75}MA_{0.25}SnI_2Br$ perovskites to better match the energy alignment and optimize carrier transport in the interface.[83] The resulting tin perovskite device delivered a high PCE of over 11% with a V_{oc} of 840 mV. On the one hand, K^+ diffused into the lattice and passivate defects in the GB. On the other hand, SCN^- anions coordinate with Sn^{2+} and restrain Sn^{2+} oxidation.

4. $HCOO^-$ and Ac^-

Pseudohalides $HCOO^-$ and Ac^- anions could affect the crystallization and optoelectronic properties of perovskites. Adding a small amount of $HCOO^-$ and Ac^- anions in precursors could achieve compact surface coverage and improve the crystallinity of perovskite thin films.[85] Interestingly, formic acid (FAH) is identified as one of the degradation products of DMF.[86] Introducing additional FAH in the precursor enables the reduction of the hydrolysis of DMF. A 70–80 mV increased V_{oc} was achieved with 7.5 vol% FAH. Increasing the acidity would raise the concentration of all solutes and decrease the strength of solvents in the precursor, thus inducing supersaturation and crystal growth.[87] Meng *et al.* observed dense nuclei with the snowflake-like crystal of FAH-induced perovskite film within 3.5 min as shown in Fig. 6a and b.[88] The control film showed almost no nucleation after the spin-coating process. Meanwhile, FAH is an ideal redox potential and has no negative effects in nucleation and crystal growth. Liu *et al.* pointed out the following reactions of FAH effect in precursor:[89]

$$HCCO^- + 2I^0 \rightarrow 2I^- + H^+ + CO_2\,(g)\uparrow \qquad (9)$$

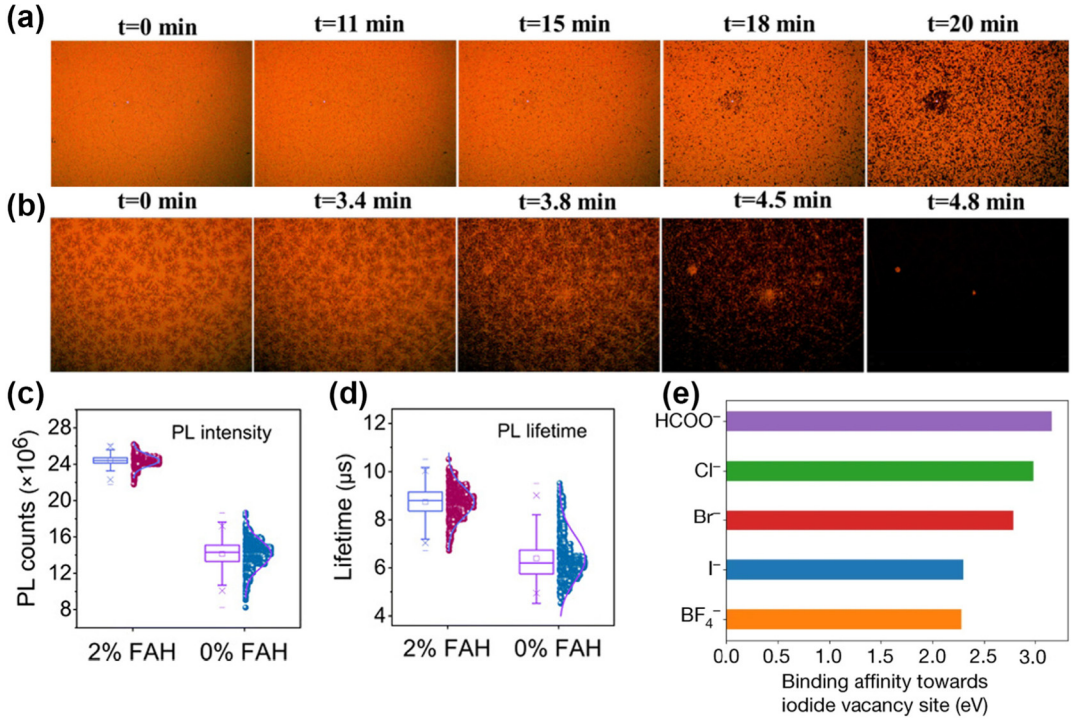

Fig. 6 (a and b) *In situ* microscopy patterns with 0 M and 0.764 M FAH-treated perovskite films. Reproduced with permission.[88] Copyright, 2020, Elsevier Publication. (c and d) PL intensities and lifetimes of perovskite films with or without FAH treatment. Reproduced with permission.[89] Copyright 2021, American Association for the Advancement of Science. (e) The interaction strengths of different anions with I^--vacancy defects at the perovskite surface. Reproduced with permission.[2] Copyright 2021, Springer Nature.

$$HCCO^- + I_3^- \rightarrow 3I^- + H^+ + CO_2\,(g)\uparrow \qquad (10)$$

$HCOO^-$ in FAH can react with adverse I^0 and form I^-, H^+, and CO_2 gas. The generated H^+ further inhibited the deprotonation of FA^+. In addition, the FAMACs films with 2 mol% FAH showed higher photoluminescence intensity (Fig. 6c) and longer lifetime (Fig. 6d). Han *et al.* further reported that FAH enhanced the crystallinity of Sn-based perovskites and exhibited high reproducibility and PCE in the corresponding devices.[90]

Estroff *et al.* first used MAFA (methylammonium formate), an ionic liquid (IL), in $MAPbI_3$ perovskites.[19] In addition to the advantages of $HCOO^-$, the property of ILs also played a key role in film growth due to their outstanding thermal stability.[16,91] Abate *et al.* indicated that the crystallization and growth process with MAFA went through the following steps:[20] (i) the coordination of Pb^{2+} and $HCOO^-$ in precursor; (ii) the HCOO-Pb bond replaced by I-Pb bond when annealing at 100 °C; (iii) complete replacement by I-Pb bond and crystal growth. The MAFA was presented at the surface in the final form. By utilizing the pseudohalide anion, Jeong *et al.* attained a certified PCE of 25.2% and remarkable operational stability over 450 h.[2] $HCOO^-$ anions showed a strong affinity with Pb^{2+} and can form a stable bonding network at the Pb^{2+}-terminated surface. As exhibited in Fig. 6e, the highest binding energy with I^- vacancies in $HCOO^-$ also proved the strong defect passivation of anion vacancies *via* strong binding affinity.

Similar to $HCOO^-$, volatile Ac^- anions also can form an intermediate with perovskite and modulate the crystallization process.[34,92] Zhou *et al.* proposed a novel strategy to suppress adverse I_2 to reduce the energy and voltage loss.[92] FAAc (formamidine acetate) as a "residual free" weak alkaline can reduce the defect density at a deep level and in particular manipulate the stoichiometry at A sites in perovskite precursors. The characteristic peak of I_2 at 360 nm showed a decreased tendency with the increasing amount of FAAc (Fig. 7a). As for the alkalinity, FAAc has a pK_a of around 7.64, whereas other alkaline additives such as NaAc (sodium acetate) and $NaHCO_3$ have a p*K*a of 9.24 and 10.33, respectively. Therefore, a large range of FAAc can regulate the absorbance of I_2 (Fig. 7b), which indicated that the weak alkaline had a great potential to regulate the α-phase perovskites on a large scale. Additionally, the volatile Ac^- facilitated grain growth with enlarged grain size and film quality. Lv *et al.* further used MAAc in the Sn–Pb perovskite precursor.[93] The strong hydrogen bonding between MAI and MAAc can not only stabilize the perovskite lattice but also increase the viscosity and solubility of the solute in the solution.

$PbAc_2$ as a pseudohalide lead source has also been attempted to improve the perovskite growth and film morphology.[15] Compared to $PbCl_2$ and PbI_2 as displayed in Fig. 7c, the perovskite film from $PbAc_2$ revealed better crystallinity. The transition process can be described as:

$$PbX_2 + 3MAI \rightarrow MAPbI_3 + 2MAX\ (X = Cl, I, Ac) \qquad (11)$$

The thermally unstable MAAc tends to evaporate more rapidly than MACl and MAI under annealing. The nucleation density with $PbAc_2$ was higher than others and the film showed full

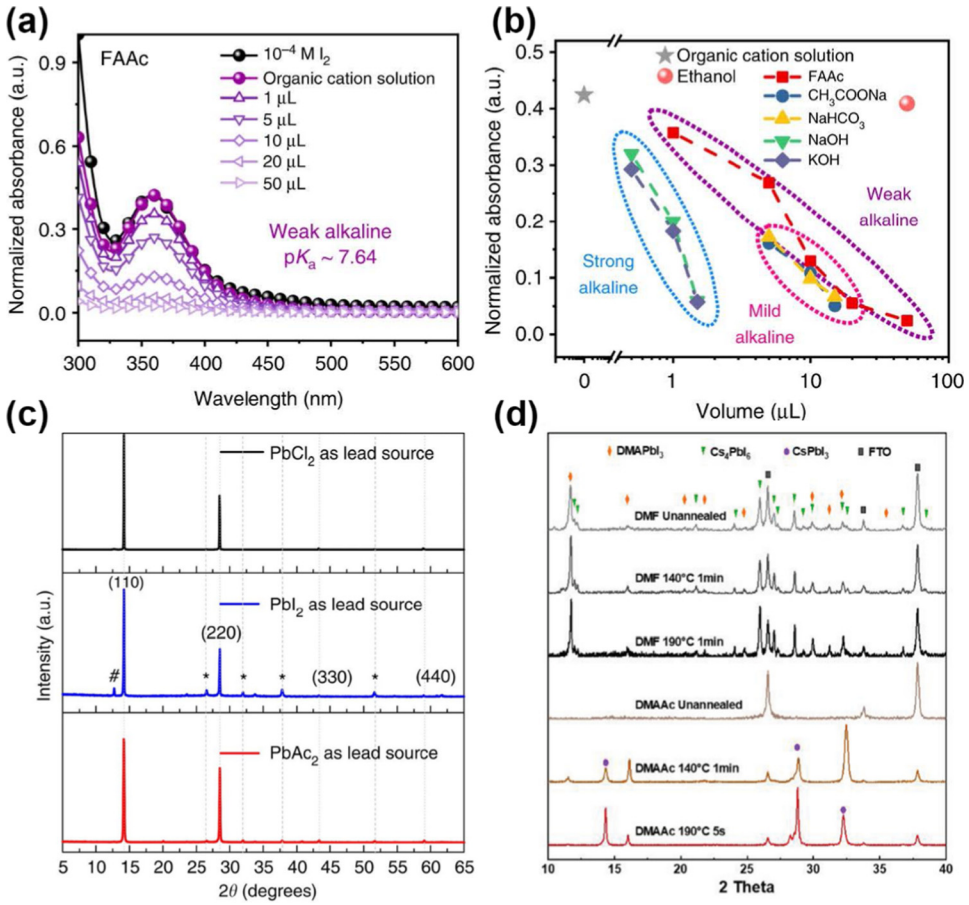

Fig. 7 (a) UV-Vis absorption of perovskite film with different amounts of FAAc. (b) Normalized absorbance with different additives. Reproduced with permission.[92] Copyright 2019, Springer Nature. (c) XRD patterns of perovskite films with $PbCl_2$, PbI_2, and $PbAc_2$ sources. Reproduced with permission.[15] Copyright 2015, Springer Nature. (d) XRD patterns of $CsPbI_3$-DMAAc precursor with different annealing times. Reproduced with permission.[94] Copyright 2022, Wiley-VCH Publication.

coverage on the substrate. Meng *et al.* eliminated the Cs_4PbI_6 intermediate phase by DMAAc (dimethylamine acetate) and stabilized the lattice structure of $DMAPbI_3$.[94] As shown in Fig. 7d, after annealing at 140 °C for 1 min, some $DMAPbI_3$ crystalline phase appeared in the absence of the Cs_4PbI_6 phase. After annealing at 190 °C for 5 s, there was no Cs_4PbI_6 phase either. Thus, the incorporation of DMAAc can shorten the crystal growth time. When annealing further, the coexisting of $DMAPbI_2Ac$ and $DMAPbI_3$ affords a dynamically stable $DMAPb(I, Ac)_3$ as follows:

$$PbI_2 + DMAAc \rightarrow DMAPbI_2Ac \quad (12)$$

$$DMAPbI_3 + DMAPbI_2Ac \rightarrow DMAPb(I,Ac)_3 \quad (13)$$

$$DMAPb(I,Ac)_3 + Cs^+ + I^- \rightarrow CaPbI_3 + DMA\,(g)\uparrow + HAc + HI\,(g)\uparrow \quad (14)$$

Therefore, DMAAc can accelerate the phase transformation from intermediate to thermally stable $CsPbI_3$ phase. Additionally, Huang *et al.* achieved a high V_{oc} up to 1.31 V and superior air stability for 4680 h with *n*-butylamine acetate (BAAc).[95] The hydrogen bonding of N–H···O=C–O$^-$ in BAAc has a stronger shielding effect than N–H···I$^-$ in BAI. The vertically aligned grains can be crystallized from the uniformly distributed intermediate.

5. BF_4^- and BH_4^-

An interesting strategy to introduce F^- in perovskite with BF_4^- anion has been investigated.[28,96–98] BF_4^- contributes to large perturbation to the electronic structure. Considering the similar ion radii of I^- and BF_4^-, Han *et al.* investigated $MAPbI_{3-x}(BF_4)_x$ perovskites with different BF_4^- concentrations.[28] All $MAPbI_{3-x}(BF_4)_x$ perovskites had the same tetragonal crystal structure like the $MAPbI_3$ perovskites. The introduction of BF_4^- leads to an obvious change in frequency-dependent electrical conductivity. In the same vein, Nagane *et al.* studied the mechanism of BF_4^- modulation *via* solid-state NMR (ssNMR) at the atomic level.[99] It was reported that BF_4^- anion was not incorporated into the perovskite lattice, but reacted with MAI like a scavenger. As shown in Fig. 8a, the F^- signal of BF_4^- was located at −147.8 ppm with a broadened signal after mixing equimolar amounts of MAI and $MABF_4$, indicating the formed $MAI\text{-}MABF_4$ cocrystal. Additionally, 10 mol% excess MAI was added with $BF_4^-$and the F^- signal was the characteristic peak

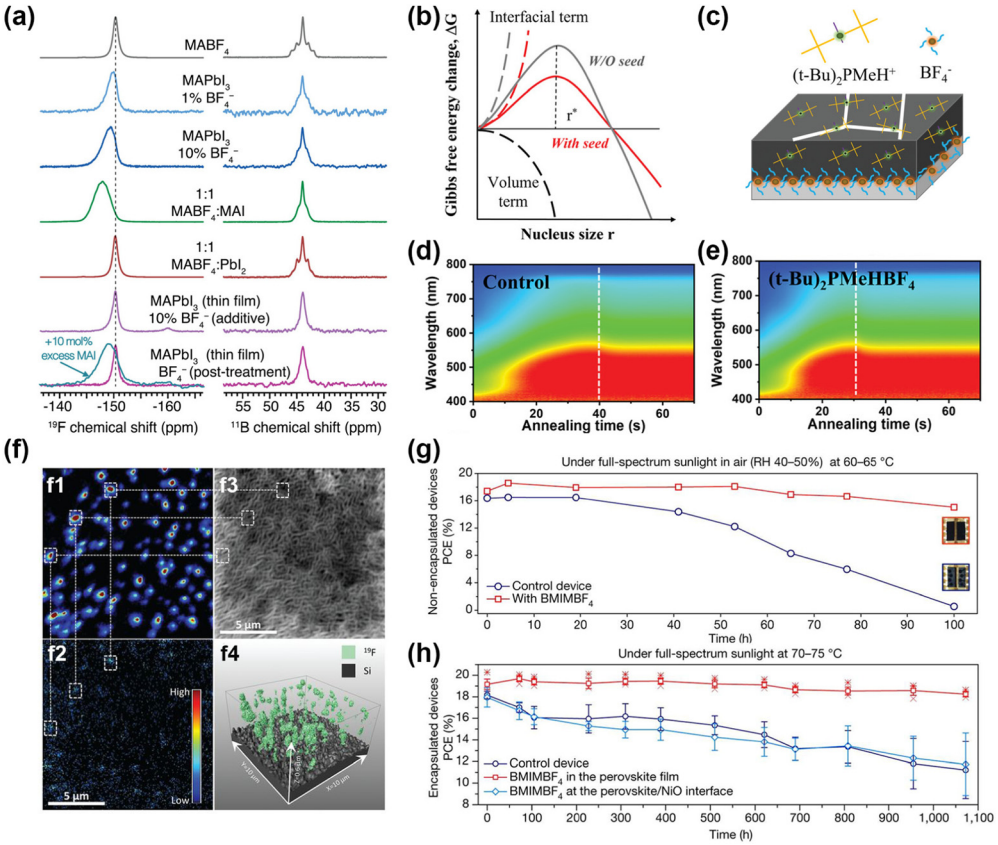

Fig. 8 (a) The ^{19}F (left) and ^{11}B NMR (right) spectra of $MABF_4$, $MAPbI_3$, $MAPbI_3$: 1% $MABF_4$, $MAPbI_3$: 10%$MABF_4$, $MABF_4$: MAI, $MABF_4$:PbI_2, and the $MAPbI_3$ film treated with 10% $MABF_4$, respectively. Reproduced with permission.[99] Copyright 2021, Wiley-VCH Publication. (b) Gibbs free energies of perovskite nucleation with or without (*t*-Bu)$_2$PMeHBF$_4$. (c) Growth modulation pattern by (*t*-Bu)$_2$PMeHBF$_4$. (d and e) *In situ* UV-Vis absorption spectra with or without (*t*-Bu)$_2$PMeHBF$_4$. Reproduced with permission.[101] Copyright 2022, Wiley-VCH Publication. (f): (f1) $^{19}F^-$ and (f2) $^{11}B^{16}O^{2-}$ anion maps for the perovskite films with $BMPBF_4$ additives. (f3) Secondary electron map for the sputtered surface morphology. (f4) 3D maps of F^- signals. Reproduced with permission.[102] Copyright 2020, American Association for the Advancement of Science. Thermal stability with (g) non-encapsulated devices and (h) encapsulated devices with or without $BMIMBF_4$ additives. Reproduced with permission.[21] Copyright 2019, Springer Nature.

of MAI-$MABF_4$ cocrystals. The δ peak at 43.9 ppm in the ^{11}B spectrum had no change in Fig. 8b, further proving that the BF_4^- was not incorporated into the perovskite lattice.

Additionally, imidazolium tetrafluoroborate ($IMBF_4$) containing imidazolium cation and BF_4^- anion to passivate the Sn–Pb perovskite was achieved by Kim *et al.*[12] The morphological effect and charge carrier dynamics with $IMBF_4$ verified the role of BF_4^- in optoelectronic properties. Meanwhile, the functional π-conjugated $QAPy^+$ (1,1′-((7,14-dioxo-7,14-dihydroquinolino[2,3-*b*]acridine-5,12-diyl)bis(octane-8,1-diyl))bis(pyridin-1-ium)) cooperating with BF_4^- lead to a higher endothermic decomposition temperature, therefore exhibiting better stability compared to the control PSCs device.[97] The $QAPyBF_4$ not only suppressed the defects of organic cation vacancies but also improved the interface contact and the adhesion of the buried interface. A signature PCE of 23.1% and V_{oc} up to 1.2 V was achieved with markedly improved thermal stability by the buried $QAPyBF_4$ interface. To demonstrate the crystallization process with BF_4^-, Zhang *et al.* applied (*t*-Bu)$_2$PMeHBF$_4$ ((*t*-Bu)$_2$PMeH$^+$ is di-*tert*-butyl(methyl)phosphonium) and analyzed the free energy in the surface/bulk by classical theory (Fig. 8b and c).[100] With the assistance of (*t*-Bu)$_2$PMeHBF$_4$, the PbI_2–(*t*-Bu)$_2$PMeBF$_4$ intermediate was prenucleated as the nucleation center and greatly reduced the interface energy. Thus, the nuclei of perovskite films can occur at a lower saturation due to the low nucleation barrier, further forming small and contact nuclei during the solvent evaporation process (Fig. 8b). Besides the faster nucleation process in the precursor, a faster crystallization process in the thin films was also observed as shown in the in-situ absorption spectra in Fig. 8d and e. The absorption signal of (*t*-Bu)$_2$PMeHBF$_4$-modified film reached the peak value 10s earlier than the control film.

Snaith *et al.* claimed that $BMPBF_4$ (BMP^+ is 1-butyl-1-methylpiperidinium) could suppress the deep trap states significantly.[21] To understand the distribution of $BMPBF_4$ in the perovskites, they utilized the nano SIMS (nanoscale secondary ion mass spectrometry) and analyzed the $^{19}F^-$ and $^{11}B^{16}O^{2-}$ signals as displayed in Fig. 8f. The $^{19}F^-$ signals were consistent with $^{11}B^{16}O^{2-}$ signals. F^- anions were distributed over the surveyed volume in the perovskite layers to play the role of defect passivation. Snaith *et al.* also incorporated $BMIMBF_4$ ($BMIM^+$ is 1-butyl-3-methylimidazolium) into perovskite layers and achieved superior long-term thermal stability both in non-encapsulated and encapsulated devices (Fig. 8g and h).[21] The $BMIM^+$ was not only located in the bulk

perovskites but also accumulated at the buried interface. However, the BF_4^- was only located at the buried interface. Both the $BMIM^+$ and BF_4^- suppressed the ion migration in the perovskite films in return.

Compared to halide anions, BH_4^- is composed of two elements and needed one extra electron for electronic shell closure.[46,103,104] The strong dihydrogen interaction between ionic hydrogen in BH_4^- and the proton hydrogen in MAI can prevent the decomposition of MAI. BH_4^- has an ion radius of 202 pm, which is similar to halides and can partially substitute these heavy halides such as I^-, Br^-, or Cl^-.[41,46] A stable $MAPbI_x(BH_4)_{3-x}$ was reported by Xu *et al.*[45] The superhalogen BH_4^- can release anion vacancies and reduce defects such as halide vacancies or organic cation vacancies by partial substitution of I^-. Sanchez-Diaz *et al.* reported the addition of $NaBH_4$ into Sn perovskites for achieving the oxidation resistance from Sn^{2+} to Sn^{4+} during the solution processing, which lead to a PCE of 10.61% with superior operational stability over 1300 h in an N_2 atmosphere.[105] The $FASnI_3$ perovskite film emerged with a compact and pinhole-free morphology with $NaBH_4$ incorporation. In this respect, this new type of superhalogen anion provides a novel design in complex perovskites.

6. PF_6^-

For the F-type superhalogen PF_6^-, it has an ion radius of 225 pm and also can be incorporated into a perovskite lattice.[41,106] Tao *et al.* achieved a PCE of 27.35% in 4T (four terminal) perovskite-Si tandem devices by F-type PF_6^- with a perovskite framework of $FA_{0.65}MA_{0.20}Cs_{0.15}Pb(I_{0.8}Br_{0.2})_{3-x}(PF_6)_x$.[106] When partial substitution of I^-/Br^- by PF_6^- occurred, the perovskite showed lattice expansion. Meanwhile, there was a released tensile strain with PF_6^- addition. Therefore, a high-quality perovskite film formed with strain relaxation, which had a positive effect on charge transport and passivation of defect density. Moreover, Hao *et al.* adopted $BMIMPF_6$ to enhance the phase stability of $CsPbI_2Br$ and delivered a PCE of 16.2% with a V_{oc} of 1.28 V.[16] The $CsPbI_2Br$ with $BMIMPF_6$ had a lower formation energy than the pure α-$CsPbI_2Br$ as shown in Fig. 9a, therefore stabilizing the α-$CsPbI_2Br$ perovskite. The average Br-I-Br angle (Fig. 9c and d) with $BMIMPF_6$ increased from 78.1° to 88.3°, thus contributing to the enhanced phase stability of α-$CsPbI_2Br$ perovskite by restraining the distortion of $[BX_6]^{4-}$ octahedrons. With KPF_6-assisted crystallization, Bu *et al.* achieved a high PCE of 23.35% in MA-free PSCs.[107] The interface between perovskite and Spiro-OMeTAD was intersected without KPF_6 treatment, whereas it had no obvious change after KPF_6 treatment as shown in cross-sectional SEM images (Fig. 9d and e). Meanwhile, PF_6^- stayed on the surface and passivated the grain boundaries and the signals of K^+ and F^- throughout the perovskite films (Fig. 9f). As a result, the device with KPF6 showed negligible ion migration after thermal aging.

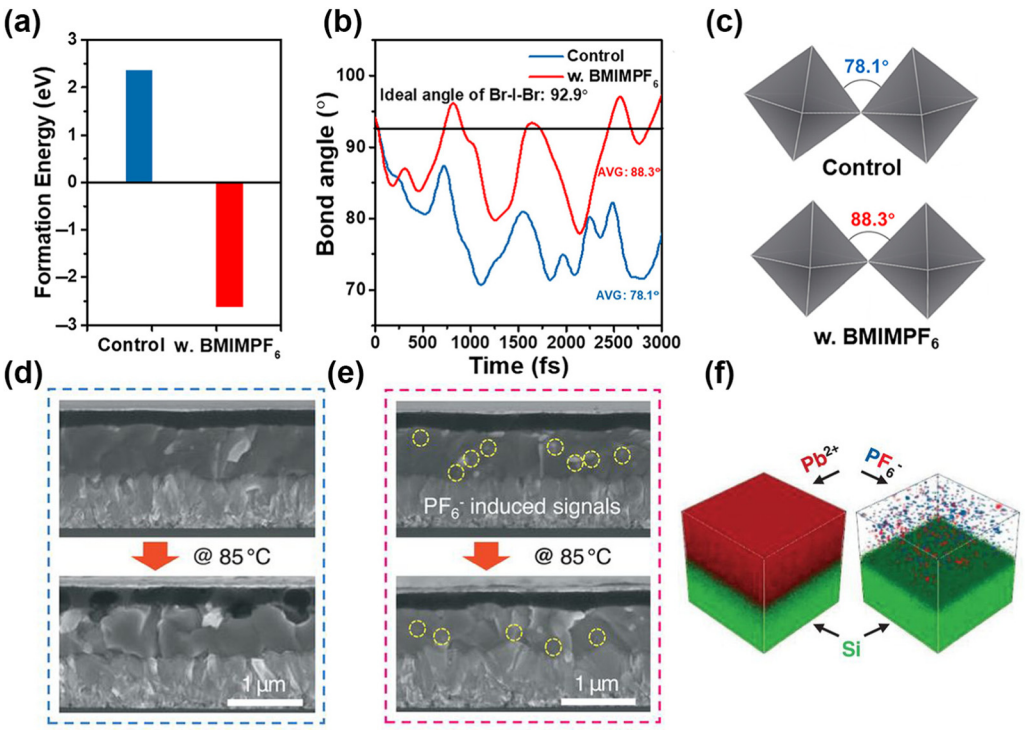

Fig. 9 (a) Formation energy of α-$CsPbI_2Br$ with or without $BMIMPF_6$ treatment. (b) Time-dependent bond angle of Br–I–Br angle and (c) the corresponding crystal schematic. Reproduced with permission.[16] Copyright 2021, Wiley-VCH Publication. Cross-sectional SEM patterns of perovskite/Spiro-OMeTAD interface (d) without and (e) with KPF_6 treatment. (f) TOF-SIMS pattern of Pb, P, and F ions in perovskites after KPF_6 addition. Reproduced with permission.[107] Copyright 2021, Springer Nature.

7. Conclusions and outlooks

The nonhalides act as emerging candidates for tuning the optoelectronic properties of perovskites and their applications in photovoltaics and beyond. The ambient light and thermal stability were greatly enhanced through this strategy. Meanwhile, they can tune the nucleation and crystal growth process and modulate the film growth process. Their positive effects on morphology, stability, electrical conductivity, carrier density, and charge transport properties provide another perspective for the future selection of the X-site anions. To achieve high-efficiency and stable PSCs with this strategy, more fundamental research studies need to be carried out.

(i) More theoretical and experimental studies should determine whether pseudohalides or superhalogens can be incorporated into a perovskite lattice. The propensity of the position in the bulk perovskite lattice or the interface/surface can offer an in depth understanding of halide management including the halide composition and halide defect regulation.

(ii) Due to the high volatile properties of SCN^-, the chemical inhomogeneity by local evaporation may be caused by unusual planar defects like edge dislocation or the bending of interlayers. The development of an elaborate vapor treatment method with SCN^- can improve the phase transition and the crystallization kinetics.

(iii) Pseudohalides contribute to enlarged grains and few boundaries with high *n*-value distribution for low-dimensional perovskites. The role of organic cations in such a system cannot be ignored. On the one hand, functionalized organic cations containing both electron-rich atoms and electron-donating chains show a strong passivation effect on the net positive charge in perovskites. On the other hand, the characteristics of the cationic component should also be investigated.

(iv) The passivation effect of $HCOO^-$ and Ac^- is mostly reflected in the halide vacancies. Meanwhile, they have a strong interaction with B-site cations to stabilize the perovskite lattice structure. The hydrogen bonding network with organic cations further enables the unique role of $HCOO^-$ and Ac^- in passivating anion-vacancy defects. Though volatile FAH and HAc have no residues in perovskite films after annealing,[85,90] long-term passivation from the precursors to thin films at high temperature is missed. Therefore, ionic liquids can be designed with various functional organic cations with pseudohalide anions in this regard. Their special properties with non-volatility and low toxicity will benefit the realization of efficient and stable PSCs.

(v) The passivation with BF_4^- or PF_6^- can mainly be embodied in blocking the invasion of H_2O and O_2, thereby facilitating moisture stability. Designing the functional hydrophilic groups with BF_4^- or PF_6^- to meet the appropriate polarity, conductivity, melting point, viscosity, and chirality is an important issue in the development of more efficient and stable PSCs soon.

Conflicts of interest

There are no conflicts to declare.

Acknowledgements

This work was financially supported by the National Key Research & Development Program of China (2022YFE0118400), the National Natural Science Foundation of China NSFC (51702038), the Science & Technology Department of Sichuan Province (2020YFG0061), and the Recruitment Program for Young Professionals. L. Ding thanks the National Key Research and Development Program of China (2017YFA0206600) and the National Natural Science Foundation of China (51773045, 21772030, 51922032, 21961160720) for financial support.

References

1 A. Kojima, K. Teshima, Y. Shirai and T. Miyasaka, Organometal Halide Perovskites as Visible-Light Sensitizers for Photovoltaic Cells, *J. Am. Chem. Soc.*, 2009, **131**, 6050–6051.
2 J. Jeong, M. Kim, J. Seo, H. Lu, P. Ahlawat, A. Mishra, Y. Yang, M. A. Hope, F. T. Eickemeyer and M. Kim, Pseudo-Halide Anion Engineering for α-$FAPbI_3$ Perovskite Solar Cells, *Nature*, 2021, **592**, 381–385.
3 S. Wang, L. Yan, W. Zhu, Z. Cao, L. Zhou, L. Ding and F. Hao, Suppressing the Formation of Tin Vacancy Yields Efficient Lead-Free Perovskite Solar Cells, *Nano Energy*, 2022, **99**, 107416.
4 F. Hao, C. C. Stoumpos, R. P. H. Chang and M. G. Kanatzidis, Anomalous Band Gap Behavior in Mixed Sn and Pb Perovskites Enables Broadening of Absorption Spectrum in Solar Cells, *J. Am. Chem. Soc.*, 2014, **136**, 8094–8099.
5 J. Liu, S. Wang, W. Zhu, Z. Tang, L. Ding and F. Hao, Highly Symmetric Lewis Base Coordinated with Sn2+ for Reducing Voltage Loss and Retarding Oxidation in Tin-Halide Perovskite Solar Cells, *Chem. Eng. J.*, 2022, 139975.
6 S. Wang, A. Wang, F. Hao and L. Ding, Renaissance of tin halide perovskite solar cells, *J. Semicond.*, 2021, **42**, 030201.
7 Y. Rong, Y. Hu, A. Mei, H. Tan, M. I. Saidaminov, S. I. Seok, M. D. McGehee, E. H. Sargent and H. Han, Challenges for Commercializing Perovskite Solar Cells, *Science*, 2018, **361**, eaat8235.
8 S. Wang, A. Wang and F. Hao, Toward stable lead halide perovskite solar cells: A knob on the A/X sites components, *iScience*, 2022, **25**, 103599.
9 W. Fu, H. Chen and A. K. Y. Jen, Two-dimensional Perovskites for Photovoltaics, *Mater. Today Nano*, 2021, **14**, 100117.
10 C. Zhang, S. Wang, X. Li, M. Yuan, L. Turyanska and X. Yang, Core/Shell Perovskite Nanocrystals: Synthesis of Highly Efficient and Environmentally Stable FAPbBr3/CsPbBr3 for LED Applications, *Adv. Funct. Mater.*, 2020, **30**, 1910582.
11 D. Cortecchia, H. A. Dewi, J. Yin, A. Bruno, S. Chen, T. Baikie, P. P. Boix, M. Grätzel, S. Mhaisalkar, C. Soci and N. Mathews, Lead-Free $MA_2CuClxBr_{4-x}$ Hybrid Perovskites, *Inorg. Chem.*, 2016, **55**, 1044–1052.

12 H. Kim, J. W. Lee, G. R. Han, S. K. Kim and J. H. Oh, Synergistic Effects of Cation and Anion in an Ionic Imidazolium Tetrafluoroborate Additive for Improving the Efficiency and Stability of Half-Mixed Pb–Sn Perovskite Solar Cells, *Adv. Funct. Mater.*, 2021, **31**, 2008801.
13 Q. Chen, H. Zhou, Y. Fang, A. Z. Stieg, T.-B. Song, H.-H. Wang, X. Xu, Y. Liu, S. Lu and J. You, The Optoelectronic Role of Chlorine in $CH_3NH_3PbI_3$ (Cl)-based Perovskite Solar Cells, *Nat. Commun.*, 2015, **6**, 1–9.
14 J. Tong, Z. Song, D. H. Kim, X. Chen, C. Chen, A. F. Palmstrom, P. F. Ndione, M. O. Reese, S. P. Dunfield and O. G. Reid, Carrier Lifetimes of >1 μs in Sn–Pb Perovskites enable Efficient All-Perovskite Tandem Solar Cells, *Science*, 2019, **364**, 475–479.
15 W. Zhang, M. Saliba, D. T. Moore, S. K. Pathak, M. T. Hörantner, T. Stergiopoulos, S. D. Stranks, G. E. Eperon, J. A. Alexander-Webber and A. Abate, Ultrasmooth Organic–Inorganic Perovskite Thin-Film Formation and Crystallization for Efficient Planar Heterojunction Solar Cells, *Nat. Commun.*, 2015, **6**, 1–10.
16 A. Wang, J. Wang, X. Niu, C. Zuo, F. Hao and L. Ding, Inhibiting Octahedral Tilting for Stable $CsPbI_2Br$ Solar Cells, *InfoMat*, 2022, **4**, e12263.
17 M. Li, C. Zhao, Z. K. Wang, C. C. Zhang, H. K. Lee, A. Pockett, J. Barbé, W. C. Tsoi, Y. G. Yang and M. J. Carnie, Interface Modification by Ionic Liquid: a Promising Candidate for Indoor Light Harvesting and Stability Improvement of Planar Perovskite Solar Cells, *Adv. Energy Mater.*, 2018, **8**, 1801509.
18 Z. Zhang, Y. Zhou, Y. Cai, H. Liu, Q. Qin, X. Lu, X. Gao, L. Shui, S. Wu and J.-M. Liu, Efficient and Stable $CH_3NH_3PbI_{3-x}(SCN)_x$ Planar Perovskite Solar Cells Fabricated in Ambient Air with Low-Temperature Process, *J. Power Sources*, 2018, **377**, 52–58.
19 D. T. Moore, K. W. Tan, H. Sai, K. P. Barteau, U. Wiesner and L. A. Estroff, Direct Crystallization Route to Methylammonium Lead Iodide Perovskite From an Ionic Liquid, *Chem. Mater.*, 2015, **27**, 3197–3199.
20 J. Y. Seo, T. Matsui, J. Luo, J. P. Correa-Baena, F. Giordano, M. Saliba, K. Schenk, A. Ummadisingu, K. Domanski and M. Hadadian, Ionic Liquid Control Crystal Growth to Enhance Planar Perovskite Solar Cells Efficiency, *Adv. Energy Mater.*, 2016, **6**, 1600767.
21 S. Bai, P. Da, C. Li, Z. Wang, Z. Yuan, F. Fu, M. Kawecki, X. Liu, N. Sakai and J. T.-W. Wang, Planar Perovskite Solar Cells with Long-Term Stability using Ionic Liquid Additives, *Nature*, 2019, **571**, 245–250.
22 D. Luo, R. Su, W. Zhang, Q. Gong and R. Zhu, Minimizing non-radiative recombination losses in perovskite solar cells, *Nat. Rev. Mater.*, 2020, **5**, 44–60.
23 Z. Cheng and J. Lin, Layered Organic–Inorganic Hybrid Perovskites: Structure, Optical Properties, Film Preparation, Patterning and Templating Engineering, *CrystEngComm*, 2010, **12**, 2646–2662.
24 M. A. Green, A. Ho-Baillie and H. J. Snaith, The Emergence of Perovskite Solar Cells, *Nat. Photonics*, 2014, **8**, 506–514.
25 A. Halder, R. Chulliyil, A. S. Subbiah, T. Khan, S. Chattoraj, A. Chowdhury and S. K. Sarkar, Pseudohalide (SCN^-)-doped $MAPbI_3$ Perovskites: A Few Surprises, *J. Phys. Chem. Lett.*, 2015, **6**, 3483–3489.
26 S. J. Kim, T. H. Lee, J.-M. Yang, J. W. Yang, Y. J. Lee, M.-J. Choi, S. A. Lee, J. M. Suh, K. J. Kwak, J. H. Baek, I. H. Im, D. E. Lee, J. Y. Kim, J. Kim, J. S. Han, S. Y. Kim, D. Lee, N.-G. Park and H. W. Jang, Vertically Aligned Two-Dimensional Halide Perovskites for Reliably Operable Artificial Synapses, *Mater. Today*, 2022, **52**, 19–30.
27 T. Wang, H. L. Loi, J. Cao, Z. Qin, Z. Guan, Y. Xu, H. Cheng, M. G. Li, C. S. Lee and X. Lu, High Open Circuit Voltage Over 1 V Achieved in Tin-Based Perovskite Solar Cells with a 2D/3D Vertical Heterojunction, *Adv. Sci.*, 2022, 2200242.
28 J. Chen, Y. Rong, A. Mei, Y. Xiong, T. Liu, Y. Sheng, P. Jiang, L. Hong, Y. Guan and X. Zhu, Hole-Conductor-Free Fully Printable Mesoscopic Solar Cell with Mixed-Anion Perovskite $CH_3NH_3PbI_{(3-x)}(BF4)_x$, *Adv. Energy Mater.*, 2016, **6**, 1502009.
29 H. Kim, J. Lim, M. Sohail and M. K. Nazeeruddin, Superhalogen Passivation for Efficient and Stable Perovskite Solar Cells, *Sol. RRL*, 2022, 2200013.
30 B. Walker, G. H. Kim and J. Y. Kim, Pseudohalides in Lead-Based Perovskite Semiconductors, *Adv. Mater.*, 2019, **31**, 1807029.
31 F. A. Mautner, R. Cortés, L. Lezama and T. Rojo, $[N(CH_3)_4][Mn(N_3)_3]$: a Compound with a Distorted Perovskite Structure through Azido Ligands, *Angew. Chem., Int. Ed. Engl.*, 1996, **35**, 78–80.
32 H. Buser, D. Schwarzenbach, W. Petter and A. Ludi, The Crystal Structure of Prussian Blue: $Fe_4[Fe(CN)_6]_3 \cdot xH_2O$, *Inorg. Chem.*, 1977, **16**, 2704–2710.
33 M.-L. Tong, J. Ru, Y.-M. Wu, X.-M. Chen, H.-C. Chang, K. Mochizuki and S. Kitagawa, Cation-Templated Construction of Three-Dimensional α-Po Cubic-Type [M(dca)3]− Networks. Syntheses, Structures and Magnetic Properties of A [M(dca)3](dca= dicyanamide; for A= benzyltributylammonium, M= Mn2+, Co2+; for A= benzyltriethylammonium, M= Mn2+, Fe2+), *New J. Chem.*, 2003, **27**, 779–782.
34 L. Duan, H. Zhang, M. Liu, M. Grätzel and J. Luo, Phase-Pure γ-$CsPbI_3$ for Efficient Inorganic Perovskite Solar Cells, *ACS Energy Lett.*, 2022, **7**, 2911–2918.
35 L. M. Castro-Castro and A. M. Guloy, Organic-Based Layered Perovskites of Mixed-Valent Gold (i)/Gold (iii) Iodides, *Angew. Chem., Int. Ed.*, 2003, **115**, 2877–2880.
36 W. Li, Z. Wang, F. Deschler, S. Gao, R. H. Friend and A. K. Cheetham, Chemically diverse and multifunctional hybrid organic–inorganic perovskites, *Nat. Rev. Mater.*, 2017, **2**, 1–18.
37 Q. Tai, P. You, H. Sang, Z. Liu, C. Hu, H. L. Chan and F. Yan, Efficient and Stable Perovskite Solar Cells Prepared in Ambient Air Irrespective of the Humidity, *Nat. Commun.*, 2016, **7**, 1–8.
38 A. M. Ganose, C. N. Savory and D. O. Scanlon, $(CH_3NH_3)2Pb(SCN)_2I_2$: A More Stable Structural Motif for

Hybrid Halide Photovoltaics?, *J. Phys. Chem. Lett.*, 2015, **6**, 4594–4598.

39 G. L. Gutsev and A. I. Boldyrev, The Electronic Structure of Superhalogens and Superalkalies, *Russ. Chem. Rev.*, 1987, **56**, 519–531.

40 S. Nagane, U. Bansode, O. Game, S. Chhatre and S. Ogale, CH3NH3PbI(3−x)(BF4)x: molecular ion substituted hybrid perovskite, *Chem. Commun.*, 2014, **50**, 9741–9744.

41 C. H. Hendon, R. X. Yang, L. A. Burton and A. Walsh, Assessment of Polyanion (BF4+ and PF6−) Substitutions in Hybrid Halide Perovskites, *J. Mater. Chem. A*, 2015, **3**, 9067–9070.

42 A. Yang, D. Li, X. Lai, H. Zhang and C. Liang, Superhalogen Boron Tetrafluoride Surface Modification Reduces the Formation of Organic Cation Vacancies on the Surface of Halide Perovskite Films, *J. Phys. Chem. C*, 2021, **125**, 21223–21233.

43 D. Li, D. Li, H. Zhang, A. Yang and C. Liang, High-Performance Photovoltaic Materials Based on the Superlattice Structures of Organic–Inorganic Halide Perovskite and Superhalogen Hybrid Perovskite, *J. Phys. Chem. Lett.*, 2020, **11**, 5282–5294.

44 C. W. F. T. Pistorius, Melting and Polymorphism of LiBH4 to 45 kbar, *Z. Phys. Chem.*, 1974, **88**, 253–263.

45 S. Xu, G. Liu, H. Zheng, X. Xu, L. Zhang, H. Xu, L. Zhu, F. Kong, Y. Li and X. Pan, Boosting Photovoltaic Performance and Stability of Super-Halogen-Substituted Perovskite Solar Cells by Simultaneous Methylammonium Immobilization and Vacancy Compensation, *ACS Appl. Mater. Interfaces*, 2020, **12**, 8249–8259.

46 P. Schouwink, M. B. Ley, A. Tissot, H. Hagemann, T. R. Jensen, Ľ. Smrčok and R. Černý, Structure And Properties of Complex Hydride Perovskite Materials, *Nat. Commun.*, 2014, **5**, 5706.

47 G. Balaji, P. H. Joshi, H. A. Abbas, L. Zhang, R. Kottokkaran, M. Samiee, M. Noack and V. L. Dalal, $CH_3NH_3PbI_3$ from Non-Iodide Lead Salts for Perovskite Solar Cells via the Formation of PbI_2, *Phys. Chem. Chem. Phys.*, 2015, **17**, 10369–10372.

48 Q. Jiang, D. Rebollar, J. Gong, E. L. Piacentino, C. Zheng and T. Xu, Pseudohalide-Induced Moisture Tolerance in Perovskite $CH_3NH_3Pb(SCN)_2I$ Thin Films, *Angew. Chem., Int. Ed.*, 2015, **127**, 7727–7730.

49 Y. Yu, C. Wang, C. R. Grice, N. Shrestha, D. Zhao, W. Liao, L. Guan, R. A. Awni, W. Meng, A. J. Cimaroli, K. Zhu, R. J. Ellingson and Y. Yan, Synergistic Effects of Lead Thiocyanate Additive and Solvent Annealing on the Performance of Wide-Bandgap Perovskite Solar Cells, *ACS Energy Lett.*, 2017, **2**, 1177–1182.

50 Y. Lou, Y. Niu, D. Yang, Q. Xu, Y. Hu, Y. Shen, J. Ming, J. Chen, L. Zhang and Y. Zhao, Rod-shaped Thiocyanate-induced Abnormal Band Gap Broadening in SCN− Doped $CsPbBr_3$ Perovskite Nanocrystals, *Nano Res.*, 2018, **11**, 2715–2723.

51 Z. Xu, M. Chen and S. F. Liu, Origin of Enhanced Stability in Thiocyanate Substituted α-$FAPbI_3$ Analogues, *Sci. China: Chem.*, 2019, **62**, 866–874.

52 M. Rameez, E. Y.-R. Lin, P. Raghunath, S. Narra, D. Song, M.-C. Lin, C.-H. Hung and E. W.-G. Diau, Development of Hybrid Pseudohalide Tin Perovskites for Highly Stable Carbon-Electrode Solar Cells, *ACS Appl. Mater. Interfaces*, 2020, **12**, 21739–21747.

53 X. Liu, K.-L. Huang, G.-M. Liang, M.-S. Wang and G.-C. Guo, Molecular Design of Luminescent Halogeno-thiocyano-d10 Metal Complexes with In Situ Formation of the Thiocyanate Ligand, *CrystEngComm*, 2009, **11**, 1615–1620.

54 F. Hao, C. C. Stoumpos, D. H. Cao, R. P. Chang and M. G. Kanatzidis, Lead-Free Solid-State Organic–Inorganic Halide Perovskite Solar Cells, *Nat. Photonics*, 2014, **8**, 489–494.

55 R. Younts, H.-S. Duan, B. Gautam, B. Saparov, J. Liu, C. Mongin, F. N. Castellano, D. B. Mitzi and K. Gundogdu, Efficient Generation of Long-Lived Triplet Excitons in 2D Hybrid Perovskite, *Adv. Mater.*, 2017, **29**, 1604278.

56 Y. Numata, Y. Sanehira, R. Ishikawa, H. Shirai and T. Miyasaka, Thiocyanate Containing Two-Dimensional Cesium Lead Iodide Perovskite, $Cs_2PbI_2(SCN)_2$: Characterization, Photovoltaic Application, and Degradation Mechanism, *ACS Appl. Mater. Interfaces*, 2018, **10**, 42363–42371.

57 Y. Li, J. Shi, H. Wu, Y. Luo, D. Li and Q. Meng, Ultra-small Interlayer Spacing and Nano Channels in Anionic Layered Perovskite $Cs_2Pb(SCN)_2I_2$ Enable Efficient Photoelectric Conversion, *Sci. China Mater.*, 2021, **64**, 61–72.

58 H. Li, X. Jiang, Q. Wei, Z. Zang, M. Ma, F. Wang, W. Zhou and Z. Ning, Low-Dimensional Inorganic Tin Perovskite Solar Cells Prepared by Templated Growth, *Angew. Chem.*, 2021, **133**, 16466–16472.

59 Z. Xu, M. Chen and S. F. Liu, Pseudohalide Induced Tunable Electronic and Excitonic Properties in Two-dimensional Single-layer Perovskite for Photovoltaics and Photoelectronic Applications, *J. Energy Chem.*, 2019, **36**, 106–113.

60 A. T. Fafarman, W.-k Koh, B. T. Diroll, D. K. Kim, D.-K. Ko, S. J. Oh, X. Ye, V. Doan-Nguyen, M. R. Crump, D. C. Reifsnyder, C. B. Murray and C. R. Kagan, Thiocyanate-Capped Nanocrystal Colloids: Vibrational Reporter of Surface Chemistry and Solution-Based Route to Enhanced Coupling in Nanocrystal Solids, *J. Am. Chem. Soc.*, 2011, **133**, 15753–15761.

61 S. Wang, C. Wu, H. Yao and F. Hao, Dimensional Tailoring Endows Tin Halide Perovskite Solar Cells with High Efficiency and Stability, *Mater. Lab.*, 2022, 220047.

62 N. D. Pham, V. T. Tiong, D. Yao, W. Martens, A. Guerrero, J. Bisquert and H. Wang, Guanidinium Thiocyanate Selective Ostwald Ripening Induced Large Grain for High Performance Perovskite Solar Cells, *Nano Energy*, 2017, **41**, 476–487.

63 J. Tong, Q. Jiang, A. J. Ferguson, A. F. Palmstrom, X. Wang, J. Hao, S. P. Dunfield, A. E. Louks, S. P. Harvey and C. Li, Carrier Control in Sn–Pb Perovskites via 2D Cation Engineering for All-Perovskite Tandem Solar Cells with

Improved Efficiency and Stability, *Nat. Energy*, 2022, **7**, 642–651.

64 W. Zhang, X. Wu, Q. Cheng, B. Wang, S. U. Zafar, B. Han, J. Zhang, H. Zhang, X. Liu and Y. Zhang, Inhibiting the Growth of 1D Intermediates in Quasi-2D Ruddlesden–Popper Perovskites, *Adv. Funct. Mater.*, 2022, 2206594.

65 J. Yang, S. C. Cho, S. Lee, J. W. Yoon, W. H. Jeong, H. Song, J. T. Oh, S. G. Lim, S. Y. Bae, B. R. Lee, M. Ahmadi, E. H. Sargent, W. Yi, S. U. Lee and H. Choi, Guanidinium-Pseudohalide Perovskite Interfaces Enable Surface Reconstruction of Colloidal Quantum Dots for Efficient and Stable Photovoltaics, *ACS Nano*, 2022, **16**, 1649–1660.

66 A. T. Fafarman, W.-k Koh, B. T. Diroll, D. K. Kim, D.-K. Ko, S. J. Oh, X. Ye, V. Doan-Nguyen, M. R. Crump and D. C. Reifsnyder, Thiocyanate-Capped Nanocrystal Colloids: Vibrational Reporter of Surface Chemistry and Solution-based Route to Enhanced Coupling in Nanocrystal Solids, *J. Am. Chem. Soc.*, 2011, **133**, 15753–15761.

67 B. Sun, O. Voznyy, H. Tan, P. Stadler, M. Liu, G. Walters, A. H. Proppe, M. Liu, J. Fan and T. Zhuang, Pseudohalide-Exchanged Quantum Dot Solids Achieve Record Auantum Efficiency in Infrared Photovoltaics, *Adv. Mater.*, 2017, **29**, 1700749.

68 H. Dong, Z. Wu, J. Xi, X. Xu, L. Zuo, T. Lei, X. Zhao, L. Zhang, X. Hou and A. K. Y. Jen, Pseudohalide-Induced Recrystallization Engineering For $CH_3NH_3PbI_3$ Film And Its Application In Highly Efficient Inverted Planar Heterojunction Perovskite Solar Cells, *Adv. Funct. Mater.*, 2018, **28**, 1704836.

69 B. Yu, J. Shi, S. Tan, Y. Cui, W. Zhao, H. Wu, Y. Luo, D. Li and Q. Meng, Efficient ($>$ 20%) and Stable All-Inorganic Cesium Lead Triiodide Solar Cell Enabled by Thiocyanate Molten Salts, *Angew. Chem., Int. Ed.*, 2021, **60**, 13436–13443.

70 B. A. Koscher, J. K. Swabeck, N. D. Bronstein and A. P. Alivisatos, Essentially Trap-Free $CsPbBr_3$ Colloidal Nanocrystals By Postsynthetic Thiocyanate Surface Treatment, *J. Am. Chem. Soc.*, 2017, **139**, 6566–6569.

71 J. T. Lin, Y. K. Hu, C. H. Hou, C. C. Liao, W. T. Chuang, C. W. Chiu, M. K. Tsai, J. J. Shyue and P. T. Chou, Superior Stability and Emission Quantum Yield (23% $\pm$ 3%) of Single-Layer 2D Tin Perovskite TEA_2SnI_4 via Thiocyanate Passivation, *Small*, 2020, **16**, 2000903.

72 X. Zhang, G. Wu, W. Fu, M. Qin, W. Yang, J. Yan, Z. Zhang, X. Lu and H. Chen, Orientation Regulation of Phenylethylammonium Cation based 2D Perovskite Solar Cell with Efficiency Higher than 11%, *Adv. Energy Mater.*, 2018, **8**, 1702498.

73 W. Li, M. U. Rothmann, Y. Zhu, W. Chen, C. Yang, Y. Yuan, Y. Y. Choo, X. Wen, Y.-B. Cheng and U. Bach, The Critical Role of Composition-Dependent Intragrain Planar Defects in The Performance of $MA_{1-x}FA_xPbI_3$ Perovskite Solar Cells, *Nat. Energy*, 2021, **6**, 624–632.

74 X. Lian, J. Chen, Y. Zhang, M. Qin, J. Li, S. Tian, W. Yang, X. Lu, G. Wu and H. Chen, Highly Efficient Sn/Pb Binary Perovskite Solar Cell via Precursor Engineering: A Two-Step Fabrication Process, *Adv. Funct. Mater.*, 2019, **29**, 1807024.

75 W. Zhang, X. Wu, J. Zhou, B. Han, X. Liu, Y. Zhang and H. Zhou, Pseudohalide-Assisted Growth of Oriented Large Grains for High-Performance and Stable 2D Perovskite Solar Cells, *ACS Energy Lett.*, 2022, **7**, 1842–1849.

76 H. Lu, Y. Liu, P. Ahlawat, A. Mishra, W. R. Tress, F. T. Eickemeyer, Y. Yang, F. Fu, Z. Wang and C. E. Avalos, Vapor-Assisted Deposition of Highly Efficient, Stable Black-Phase FAPbI3 Perovskite Solar Cells, *Science*, 2020, **370**, eabb8985.

77 D. Kim, H. J. Jung, I. J. Park, B. W. Larson, S. P. Dunfield, C. Xiao, J. Kim, J. Tong, P. Boonmongkolras and S. G. Ji, Efficient, Stable Silicon Tandem Cells Enabled by Anion-Engineered Wide-Bandgap Perovskites, *Science*, 2020, **368**, 155–160.

78 D. B. Khadka, Y. Shirai, M. Yanagida and K. Miyano, Pseudohalide Functional Additives in Tin Halide Perovskite for Efficient and Stable Pb-Free Perovskite Solar Cells, *ACS Appl. Energy Mater.*, 2021, **4**, 12819–12826.

79 D. Yu, Q. Wei, H. Li, J. Xie, X. Jiang, T. Pan, H. Wang, M. Pan, W. Zhou, W. Liu, P. C. Y. Chow and Z. Ning, Quasi-2D Bilayer Surface Passivation for High Efficiency Narrow Bandgap Perovskite Solar Cells, *Angew. Chem., Int. Ed.*, 2022, **61**, e202202346.

80 N. Yarita, H. Tahara, M. Saruyama, T. Kawawaki, R. Sato, T. Teranishi and Y. Kanemitsu, Impact of Postsynthetic Surface Modification on Photoluminescence Intermittency in Formamidinium Lead Bromide Perovskite Nanocrystals, *J. Phys. Chem. Lett.*, 2017, **8**, 6041–6047.

81 F. Xu, J. Liu, A. S. Subbiah, W. Liu, J. Kang, G. T. Harrison, X. Yang, F. H. Isikgor, E. Aydin, M. De Bastiani and S. De Wolf, Potassium Thiocyanate-Assisted Enhancement of Slot-Die-Coated Perovskite Films for High-Performance Solar Cells, *Small Sci.*, 2021, **1**, 2000044.

82 C. Zheng, C. Bi, F. Huang, D. Binks and J. Tian, Stable and Strong Emission $CsPbBr_3$ Quantum Dots by Surface Engineering for High-Performance Optoelectronic Films, *ACS Appl. Mater. Interfaces*, 2019, **11**, 25410–25416.

83 J.-J. Cao, Y.-H. Lou, W.-F. Yang, K.-L. Wang, Z.-H. Su, J. Chen, C.-H. Chen, C. Dong, X.-Y. Gao and Z.-K. Wang, Multifunctional Potassium Thiocyanate Interlayer for Eco-Friendly Tin Perovskite Indoor and Outdoor Photovoltaics, *Chem. Eng. J.*, 2022, **433**, 133832.

84 Q. Chen, J. Wu, J. T. Matondo, L. Bai, D. M. Maurice and M. Guli, Optimization of Bulk Defects in Sn/Pb Mixed Perovskite Solar Cells Through Synergistic Effect of Potassium Thiocyanate, *Sol. RRL*, 2020, **4**, 2000584.

85 Y. Su, J. Yang, G. Liu, W. Sheng, J. Zhang, Y. Zhong, L. Tan and Y. Chen, Acetic Acid-Assisted Synergistic Modulation of Crystallization Kinetics and Inhibition of Sn2+ Oxidation in Tin-Based Perovskite Solar Cells, *Adv. Funct. Mater.*, 2022, **32**, 2109631.

86 N. K. Noel, M. Congiu, A. J. Ramadan, S. Fearn, D. P. McMeekin, J. B. Patel, M. B. Johnston, B. Wenger and H. J. Snaith, Unveiling The Influence of pH on The

Crystallization of Hybrid Perovskites, Delivering Low Voltage Loss Photovoltaics, *Joule*, 2017, **1**, 328–343.

87 P. K. Nayak, D. T. Moore, B. Wenger, S. Nayak, A. A. Haghighirad, A. Fineberg, N. K. Noel, O. G. Reid, G. Rumbles and P. Kukura, Mechanism For Rapid Growth of Organic–Inorganic Halide Perovskite Crystals, *Nat. Commun.*, 2016, **7**, 1–8.

88 L. Meng, Q. Wei, Z. Yang, D. Yang, J. Feng, X. Ren, Y. Liu and S. Liu, Improved Perovskite Solar Cell Efficiency by Tuning The Colloidal Size and Free Ion Concentration in Precursor Solution Using Formic Acid Additive, *J. Energy Chem.*, 2020, **41**, 43–51.

89 Y. Liu, Y. Zhang, X. Zhu, Z. Yang, W. Ke, J. Feng, X. Ren, K. Zhao, M. Liu and M. G. Kanatzidis, Inch-Sized High-Quality Perovskite Single Crystals by Suppressing Phase Segregation for Light-Powered Integrated Circuits, *Sci. Adv.*, 2021, **7**, eabc8844.

90 X. Meng, T. Wu, X. Liu, X. He, T. Noda, Y. Wang, H. Segawa and L. Han, Highly Reproducible and Efficient $FASnI_3$ Perovskite Solar Cells Fabricated with Volatilizable Reducing Solvent, *J. Phys. Chem. Lett.*, 2020, **11**, 2965–2971.

91 A. Wang, X. Deng, J. Wang, S. Wang, X. Niu, F. Hao and L. Ding, Ionic Liquid Reducing Energy Loss and Stabilizing $CsPbI_2Br$ Solar Cells, *Nano Energy*, 2021, **81**, 105631.

92 Y. Chen, N. Li, L. Wang, L. Li, Z. Xu, H. Jiao, P. Liu, C. Zhu, H. Zai and M. Sun, Impacts of Alkaline on The Defects Property and Crystallization Kinetics in Perovskite Solar Cells, *Nat. Commun.*, 2019, **10**, 1–10.

93 S. Lv, W. Gao, G. Xing, L. Chao, L. Song, M. Li, L. Fu, Y. Chen and C. Ran, Improving the Air Resistance of the Precursor Solution for Ambient-Air Coating of an Sn–Pb Perovskite Film with Superior Photovoltaic Performance, *ACS Appl. Mater. Interfaces*, 2022, **14**, 43362–43371.

94 Y. Cui, J. Shi, F. Meng, B. Yu, S. Tan, S. He, C. Tan, Y. Li, H. Wu, Y. Luo, D. Li and Q. Meng, A Versatile Molten-Salt Induction Strategy to Achieve Efficient CsPbI3 Perovskite Solar Cells with a High Open-Circuit Voltage >1.2 V, *Adv. Mater.*, 2022, 2205028.

95 C. Liang, H. Gu, Y. Xia, Z. Wang, X. Liu, J. Xia, S. Zuo, Y. Hu, X. Gao and W. Hui, Two-dimensional Ruddlesden–Popper layered Perovskite Solar Cells Based on Phase-Pure Thin Films, *Nat. Energy*, 2021, **6**, 38–45.

96 S. Nagane, U. Bansode, O. Game, S. Chhatre and S. Ogale, $CH_3NH_3PbI_{(3-x)}(BF4)_x$: Molecular Ion Substituted Hybrid Perovskite, *Chem. Commun.*, 2014, **50**, 9741–9744.

97 J. Zhang, S. Wu, T. Liu, Z. Zhu and A. K. Y. Jen, Boosting Photovoltaic Performance for Lead Halide Perovskites Solar Cells with BF_4^- anion Substitutions, *Adv. Funct. Mater.*, 2019, **29**, 1808833.

98 H. Zhang, S. Xu, T. Guo, D. Du, Y. Tao, L. Zhang, G. Liu, X. Chen, J. Ye, Z. Guo and H. Zheng, Dual Effect of Superhalogen Ionic Liquids Ensures Efficient Carrier Transport for Highly Efficient and Stable Perovskite Solar Cells, *ACS Appl. Mater. Interfaces*, 2022, **14**, 28826–28833.

99 S. Nagane, S. Macpherson, M. A. Hope, D. J. Kubicki, W. Li, S. D. Verma, J. Ferrer Orri, Y.-H. Chiang, J. L. MacManus-Driscoll, C. P. Grey and S. D. Stranks, Tetrafluoroborate-Induced Reduction in Defect Density in Hybrid Perovskites through Halide Management, *Adv. Mater.*, 2021, **33**, 2102462.

100 H. Zhang, Z. Ren, K. Liu, M. Qin, Z. Wu, D. Shen, Y. Zhang, H. T. Chandran, J. Hao, C.-S. Lee, X. Lu, Z. Zheng, J. Huang and G. Li, Controllable Heterogenous Seeding-Induced Crystallization for High-Efficiency $FAPbI_3$-Based Perovskite Solar Cells Over 24%, *Adv. Mater.*, 2022, **34**, 2204366.

101 H. Zhang, Z. Ren, K. Liu, M. Qin, Z. Wu, D. Shen, Y. Zhang, H. T. Chandran, J. Hao and C. S. Lee, Controllable Heterogenous Seeding-Induced Crystallization for High-Efficiency $FAPbI_3$-Based Perovskite Solar Cells Over 24%, *Adv. Mater.*, 2022, **34**, 2204366.

102 Y.-H. Lin, N. Sakai, P. Da, J. Wu, H. C. Sansom, A. J. Ramadan, S. Mahesh, J. Liu, R. D. J. Oliver, J. Lim, L. Aspitarte, K. Sharma, P. K. Madhu, A. B. Morales-Vilches, P. K. Nayak, S. Bai, F. Gao, C. R. M. Grovenor, M. B. Johnston, J. G. Labram, J. R. Durrant, J. M. Ball, B. Wenger, B. Stannowski and H. J. Snaith, A Piperidinium Salt Stabilizes Efficient Metal-Halide Perovskite Solar Cells, *Science*, 2020, **369**, 96–102.

103 G. L. Gutsev and A. I. Boldyrev, DVM-Xα Calculations on The Ionization Potentials of MX_{k+1}^- Complex Anions and The Electron Affinities of MX_{k+1} ''superhalogens'', *Chem. Phys.*, 1981, **56**, 277–283.

104 H. Fang and P. Jena, Super-Ion Inspired Colorful Hybrid Perovskite Solar Cells, *J. Mater. Chem. A*, 2016, **4**, 4728–4737.

105 J. Sanchez-Diaz, R. S. Sánchez, S. Masi, M. Krecmarová, A. O. Alvarez, E. M. Barea, J. Rodriguez-Romero, V. S. Chirvony, J. F. Sánchez-Royo, J. P. Martinez-Pastor and I. Mora-Seró, Tin Perovskite Solar Cells with $>1{,}300$ h of Operational Stability in N2 through A Synergistic Chemical Engineering Approach, *Joule*, 2022, **6**, 861–883.

106 J. Tao, X. Liu, J. Shen, S. Han, L. Guan, G. Fu, D.-B. Kuang and S. Yang, F-Type Pseudo-Halide Anions for High-Efficiency and Stable Wide-Band-Gap Inverted Perovskite Solar Cells with Fill Factor Exceeding 84%, *ACS Nano*, 2022, **16**, 10798–10810.

107 T. Bu, J. Li, H. Li, C. Tian, J. Su, G. Tong, L. K. Ono, C. Wang, Z. Lin and N. Chai, Lead Halide–Templated Crystallization of Methylamine-Free Perovskite for Efficient Photovoltaic Modules, *Science*, 2021, **372**, 1327–1332.